

# Tac2Pose: Tactile Object Pose Estimation from the First Touch.

Maria Bauza\*, Antonia Bronars\*, and Alberto Rodriguez

## Abstract

In this paper, we present Tac2Pose, an object-specific approach to tactile pose estimation from the first touch for known objects. Given the object geometry, we learn a tailored perception model in simulation that estimates a probability distribution over possible object poses given a tactile observation. To do so, we simulate the contact shapes that a dense set of object poses would produce on the sensor. Then, given a new contact shape obtained from the sensor, we match it against the pre-computed set using an object-specific embedding learned using contrastive learning. We obtain contact shapes from the sensor with an object-agnostic calibration step that maps RGB tactile observations to binary contact shapes. This mapping, which can be reused across object and sensor instances, is the only step trained with real sensor data. This results in a perception model that localizes objects from the first real tactile observation. Importantly, it produces pose distributions and can incorporate additional pose constraints coming from other perception systems, multiple contacts, or priors.

We provide quantitative results for 20 objects. Tac2Pose provides high accuracy pose estimations from distinctive tactile observations while regressing meaningful pose distributions to account for those contact shapes that could result from different object poses. We extend and test Tac2Pose in multi-contact scenarios where two tactile sensors are simultaneously in contact with the object, as during a grasp with a parallel jaw gripper. We further show that when the output pose distribution is filtered with a prior on the object pose, Tac2Pose is often able to improve significantly on the prior. This suggests synergistic use of Tac2Pose with additional sensing modalities (e.g. vision) even in cases where the tactile observation from a grasp is not sufficiently discriminative. Given a coarse estimate of an object's pose, even ambiguous contacts can be used to determine an object's pose precisely.

We also test Tac2Pose on object models reconstructed from a 3D scanner, to evaluate the robustness to uncertainty in the object model. We show that even in the presence of model uncertainty, Tac2Pose is able to achieve fine accuracy comparable to when the object model is the manufacturer's CAD model. Finally, we demonstrate the advantages of Tac2Pose compared with three baseline methods for tactile pose estimation: directly regressing the object pose with a neural network, matching an observed contact to a set of possible contacts using a standard classification neural network, and direct pixel comparison of an observed contact with a set of possible contacts.

Website: [mcube.mit.edu/research/tac2pose.html](https://mcube.mit.edu/research/tac2pose.html)

## Keywords

Tactile Sensing, Object Pose Estimation, Manipulation, Perception, Machine Learning, Grasping, Contrastive Learning

## 1 Introduction

Robotics history sends a clear lesson: accurate and reliable perception is an enabler of progress in robotics. From depth cameras to convolutional neural networks, we have seen how advances in perception foster the development of new techniques and applications. For instance, the invention of high-resolution LIDAR fueled self-driving cars, and the generalization capacity of deep neural networks has dominated progress in perception and grasp planning in warehouse automation (Zeng et al. 2018; Milan et al. 2018; Schwarz et al. 2018). The long term goal of our research is to understand the key role that tactile sensing plays in that progress. In particular, we are interested in robotic manipulation applications, where occlusions challenge accurate object pose estimation, and where object dynamics are dominated by contact interactions.

In this paper, we propose Tac2Pose, a framework to estimate the pose of a touched object, as illustrated in Figure 1. Given a 3D model of the object, Tac2Pose learns an object-specific perception model in simulation, tailored

at estimating the pose of the object from one—or possibly multiple—tactile images. As a result, the approach localizes the object from the first touch, i.e., without requiring any previous interaction. The perception model is based on merging two key ideas:

- *Geometric contact rendering*: we use the object model to render the contact shapes that the tactile sensor would observe for a dense set of contact poses.
- *Contact shape matching*: given the estimated contact shape from a tactile observation, we match it

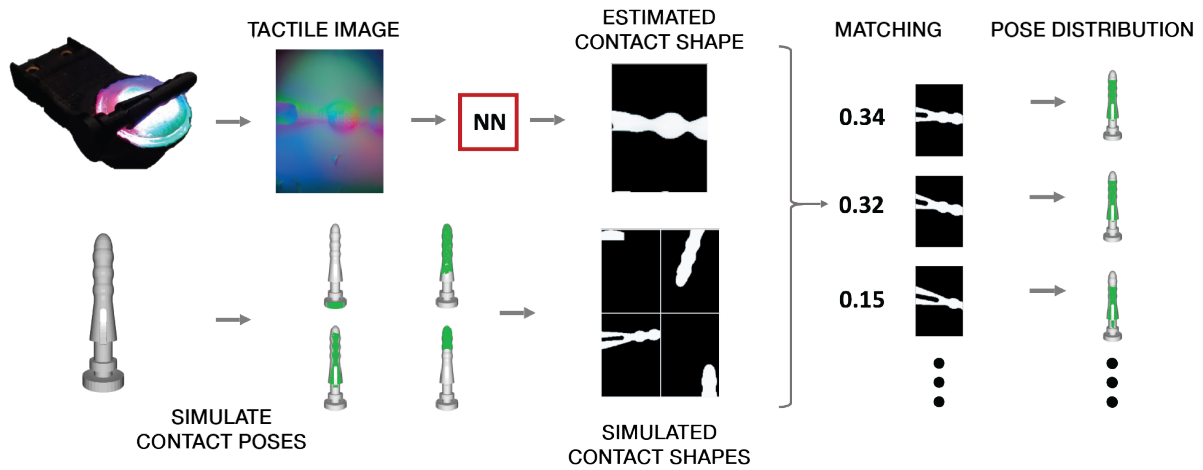
Massachusetts Institute of Technology, Cambridge, MA 02139, USA

\* Authors with equal contribution.

### Corresponding author:

Maria Bauza,  
Massachusetts Institute of Technology, Cambridge, MA 02139, USA.  
Email: [bauza@mit.edu](mailto:bauza@mit.edu)

This paper extends the paper that appeared in the proceedings of the 2020 Conference on Robot Learning Bauza et al. (2020).



**Figure 1. Tactile pose estimation with Tac2Pose.** (Bottom row) In simulation, we render geometric contact shapes of the object from a dense set of possible contacts between object and tactile sensor. (Top row) The real sensor generates a tactile image from which we estimate its geometric contact shape. We then match it against the simulated set of contact shapes to find the distribution of contact poses that are more likely to have generated it. For efficiency and robustness, we do the contact shape matching in an embedding learned for that particular object.

against a precomputed dense set of simulated contact shapes. The comparison happens in an object-specific embedding for contact shapes learned in simulation using contrastive learning tools (He et al. 2019). This provides robustness and speed compared to other methods based on direct pixel comparisons.

Enabled by the discriminative power of tactile sensing, the proposed approach is motivated by scenarios where the main requirement is estimation accuracy and where object models will be available beforehand. Many industrial scenarios fit this category. We also consider cases where the object model is not known exactly, but reconstructed apriori with a 3D scanner. This broadens the set of scenarios to which Tac2Pose can be applied. Many previous solutions to tactile pose estimation require prior exploration of the object (Li et al. 2014; Bauza et al. 2019). Acquiring this tactile experience can be expensive, and in many cases, unrealistic. In this paper, instead, we learn the perception model directly from the object mesh model. The results in Sec. 4.2 show that the model learned in simulation directly transfers to the real world.

We attribute this to the object-specific nature of the learned model, the high resolution nature of the tactile sensors, and the contrastive-based perception framework. Tac2Pose uses an intermediate representation of the tactile image, a binary contact mask, which we are able to generate with high fidelity both in simulation and using the real sensor. Furthermore, because Tac2Pose matches observed contact shapes to a discrete set of simulated contacts, the match doesn't need to be perfect - just better than the other possible options - for the localization to be accurate.

Also key to the approach is that, by simulating a dense set of tactile imprints, the algorithm can reason over pose distributions, not only the best estimate. The learned embedding allows us to efficiently compute the likelihood of each contact shape in the simulated dense set to match with the predicted contact shape from the tactile sensor. Predicting distributions is key given that tactile sensing provides local

observations, which often do not discriminate pose globally (see, for example, the first contact in Figure 7a).

Finally, by maintaining probability distributions in pose space, we can incorporate extra constraints over the likelihood of each pose. We illustrate it in the case of multi-contact, where information from multiple tactile observations must be combined simultaneously, and in the case of filtering the distribution with a prior estimate of the object pose. In practice, this prior estimate could come from previous tactile observations, kinematics, or other perception systems (e.g., vision).

We evaluate the performance of Tac2Pose on real datasets collected for 20 different real objects of varying size and complexity in Section 4.2. The labelled datasets evaluated in this work are available on the project website. For 5 of the 20 objects, we also reconstruct the object models using a 3D scanner. We compare the localization accuracy on the same real datasets, when using a reconstructed model versus the manufacturer's CAD model, in Section 4.3.

Finally, we compare the performance of Tac2Pose with three baseline methods for 5 objects in Section 4.4: direct regression of the object pose using a neural network, matching an observed contact to a set of possible contacts using a standard classification network, and matching an observed contact to a set of possible contacts using direct pixel comparison.

In summary, the main contribution of this work is a framework for tactile pose estimation for objects with known geometry, with the following primary strengths:

1. Provides accurate pose estimation from the first touch, without requiring any previous interactions with the object.
2. Reasons over pose distributions by efficiently computing probabilities between a real contact shape and a dense set of simulated contact shapes. This allows for integration of pose constraints, such as those arising from multi-contact scenarios or prior estimates of the object pose.

We evaluate Tac2Pose’s accuracy with respect to object geometry, uncertainty (from reconstructed object geometry and tactile sensor noise), and other methods for tactile localization. In particular, we show:

1. Quantitative results for 20 objects on three ablations of Tac2Pose using real data: single contact, parallel jaw grasping, and parallel jaw grasping with a pose prior (Section 4.2). We achieve high localization accuracy when making contact with distinct object features. Complete results for each object can be seen in Table 1.
2. Comparisons for results on 5 objects using reconstructed object shapes instead of manufacturer’s CAD models (Section 4.3). The localization error on reconstructed models increases between 0.2 to 1.5mm compared to manufacturer’s CAD models. Complete results can be seen in Table 2.
3. Better performance of Tac2Pose when compared with three baseline methods (Section 4.4). Results on real contact shapes for 5 objects can be seen in Table 4.

Finally, this paper extends our previous work on tactile localization (Bauza et al. 2020) in several ways. First we provide results for 20 different objects (instead of 4) and analyze Tac2Pose in the case of a single contact, as well as when localizing objects using the two contacts from a parallel-jaw grasp, or when there is a prior pose distribution (that could come from vision). Moreover, we also greatly expand the number of possible contacts that we test per object, and the generality of grids that we match against, which simulates more closely a scenario with truly no prior information. This work also includes comparisons against sensible baselines, uses a better sensor and novel algorithm for extracting contact masks. Finally, we provide extensive details over the existence of non-unique contacts, the importance of 3D models (by analyzing the effect of using reconstructed rather than perfect object models), and quality of the resulting pose distributions, which further exposes the complexity of solving tactile localization.

## 2 Related Work

Tactile sensing has been extensively explored in the robotics community. Relevant to this paper, this has resulted in the development of high-resolution tactile sensors and their use in a wide range of robotic manipulation applications. In this section, we review works that study tactile pose estimation and refer the reader to (Luo, Bimbo, Dahiya and Liu 2017) for a more in-depth review of other applications of tactile sensing.

While we propose to use high-resolution tactile sensors that are discriminative and rich in contact information, most initial works in tactile localization were focused on low-resolution tactile sensors (Schaeffer and Okamura 2003; Corcoran 2010; Petrovskaya and Khatib 2011; Chalon et al. 2013; Bimbo et al. 2016; Saund et al. 2017; Javdani et al. 2013; Chebotar et al. 2014). Some works explore how to combine multiple tactile readings and reason in the space of contact manifolds (Koval et al. 2017, 2015). However, these

are based on binary contact/no-contact signals, and require many tactile readings to narrow pose estimates.

Given the challenges from the locality of tactile sensing, recent works have gravitated towards two different approaches. Combining tactile and vision to obtain better global estimates of the object pose or using higher-resolution tactile sensors that can better discriminate different contacts. Among the solutions that combine vision and tactile, most rely on tactile sensors as binary contact detectors whose main purpose is to refine the predictions from vision (Bimbo et al. 2015; Allen et al. 1999; Ilonen et al. 2014; Falco et al. 2017; Yu and Rodriguez 2018).

Other works, more in line with Tac2Pose, have focused on using high-resolution tactile sensors as the main sensing source for object localization. Initial works in this direction used image-based tactile sensors to recover the contact shape of an object and then use it to filter the object pose (Platt et al. 2011; Pezzementi et al. 2011; Luo, Mou, Althoefer and Liu 2017). However, these approaches only provide results on planar objects and require previous tactile exploration. There has also been some recent work on highly deformable tactile sensors for object localization (Kuppuswamy et al. 2019). These sensors are large enough to fully cover the touched objects, which eases localization.

In this work, we use the image-based tactile sensor GelSlim 3.0 (Taylor et al. 2021). The sensing capabilities of high-resolution sensors of this kind have already proven useful in multiple robotic applications, including assessing grasp quality (Hogan et al. 2018), improving 3D shape perception (Wang et al. 2018) or directly learning from tactile images how to do contour following (Lepora et al. 2019) or tactile servoing (Tian et al. 2019).

For the task of tactile object localization, Li et al. (2014) proposed to extract local contact shapes from objects to build a map of the object and then use it to localize new contacts. The approach is meant to deal with small parts with discriminative features. Later Izatt et al. (2017) proposed to compute pointclouds from the sensor and use them to complement a vision-based tracker. Their tracker is fused with vision to deal with the uncertainty that arises from the locality of tactile sensing. In previous work (Bauza et al. 2019), we proposed to extract local contact shapes from the sensors and match them to the tactile map of the objects to do object pose estimation. This approach requires the estimation of a tactile map for each object by extensively exploring them with the sensor.

Sodhi et al. (2020) estimated object pose during planar pushing from a stream of tactile imprints through a factor graph-based estimation framework. Their tactile observation model is trained to predict the relative pose of the object between a pair of non-sequential tactile images. This approach is designed to track the drift of an object from an initial well-known pose. Similarly, Sodhi et al. (2021) estimated 3D object pose over a contact sequence through a factor graph-based estimation framework. The tactile observation model maps from tactile images to surface normals using an image-to-image translation network, and uses ICP to determine the relative pose between 3D contact geometry in a contact sequence. This approach is designed to track the drift of object from an initial well-known pose, where the object itself is arbitrary and unknown. In

comparison, Tac2Pose assumes known object geometry and estimates the pose of the object from scratch, while also being able to exploit prior information when available.

Tac2Pose moves all object-specific computations to simulation and only requires an object-agnostic calibration step of the tactile sensor to predict contact shapes from RGB images from the GelSlim sensor (Bauza et al. 2020). As a result, we can render in simulation contact shapes and learn object-specific models for pose estimation that translate well to the real world and achieve good accuracy from the first contact.

Recent work on tactile sensing applied to object insertion (Kim and Rodriguez 2021) also uses an intermediate representation of the tactile image as the input to their insertion policy. Because this intermediate representation (pose of the contact line between the object and the cavity during an insertion attempt) can be simulated easily, the insertion policy can be trained entirely in simulation. Both this work and ours demonstrate the value of relying on geometric intermediate representations of contact shapes to allow high fidelity transfer of models trained on simulated data to real robotic systems.

Finally, Tac2Pose to tactile pose estimation is related to methods recently explored in the computer vision community where they render realistic images of objects and learn how to estimate the orientation of an object given a new image of it (Sundermeyer et al. 2018; Jeon and Kim 2020). Li et al. (2018) designs a network to predict a relative pose between an observed image, and a rendered image of the object in a known pose. The method is used to iteratively improve on a coarse initial estimate of object pose. Labbé et al. (2020) leverages a modified version of Li et al. (2018) to estimate the pose of multiple known objects from a sequence of images from multiple, unknown, viewpoints. The approach consists of predicting object poses relative to the camera within single views, then robustly matching objects and poses between views, before performing a scene-level refinement of both object and camera pose. Although this method does not reason explicitly over pose distributions for a single-view estimate of pose, it is able to handle occlusions and inaccurate single estimates by combining information from multiple viewpoints.

Other methods address occlusion and inaccurate estimates by reasoning over pose distributions directly. Deng et al. (2019) estimates the 6D pose (3D translation, and a distribution over a discretization of 3D rotations) of an object in a Rao-Blackwellized particle filtering framework. The distributions generated using this method function as scores on a codebook of possible poses, rather than as well-defined probability distributions. Tac2Pose, in contrast, regresses probability distributions which can be combined with distributions coming from additional contacts, sensing modalities, or priors.

### 3 Method

We present an approach to object pose estimation based on tactile sensing and known object models; illustrated in Fig. 1. In an object-specific embedding, we match a dense set of simulated *contact shapes* against the estimated contact shape from a real tactile observation. A contact shape is a binary mask over contact regions on the tactile sensor. This results

in a probability distribution over contact poses that can be later refined using other pose constraints. For example, we can combine information from the two contact shapes and the gripper opening obtained by grasping an object with a parallel jaw gripper.

We predict real contact shapes directly from the raw RGB tactile images that the sensor outputs (Section 3.1). As seen in the top left quadrant of Figure 1, we predict a binary mask over the region of contact (a.k.a. the contact shape) from an RGB tactile image with high fidelity.

The next steps of Tac2Pose exploit the object model to estimate the contact pose, and are learned in simulation without using any real tactile observations. First, we render the contact shape for a given object pose, using the object model (Section 3.2). Examples of the correspondence between object pose and contact shape obtained through geometric contact rendering can be seen in the bottom half of Figure 1. Next, we use geometric contact rendering to generate a dense set of object poses and their respective contact shapes, and use contrastive learning to learn an embedding to match contact shapes depending on the closeness of their object poses (Section 3.3). As a result, given the estimated contact shape from a real tactile observation, we can match it against this pre-computed dense set to obtain a probability distribution over contact poses.

To predict contact poses beyond the resolution of the pre-computed set, it is possible to combine Tac2Pose with registration techniques on the contact shapes. While we do not explore this refinement step in detail in this paper, we showed preliminary results on the efficacy of using FilterReg (Gao and Tedrake 2019) to further increase the localization resolution in (Bauza et al. 2020). Finally, because our perception model outputs distributions over contact poses, is not restricted to single tactile observations. The distribution can be filtered or combined with other information coming from multi-contact scenarios, other sensing modalities, or additional pose constraints (Section 3.4).

#### 3.1 Contact shape prediction from tactile observations

Given a tactile observation, our goal is to extract the contact shape that produces it. To that aim, we train an image translation network (pix2pix) based on Isola et al. (2018) to map RGB tactile observations to contact shapes. We train pix2pix using pairs of real RGB tactile images and their corresponding contact shapes. The training data is collected autonomously in a controlled 4-axis stage that generates planned touches on known 3D-printed shapes, following the approach proposed in Bauza et al. (2019). The dataset we use to train pix2pix contains 10,000 RGB tactile image/contact shape pairs from 32 distinct contact geometries. The dataset does not contain examples of contact geometries from any of the objects we use to evaluate tactile localization in Section 4.1. Note that the map between RGB tactile images and contact shapes is independent of the object, and therefore we only need to gather labelled data once. Empirically, we found that a model trained on images from a single GelSlim sensor generalizes well across multiple instances of GelSlim sensors.



We provide further implementation details in Section A of the Appendix, including visualizations of the 32 contact geometries used for training (Figure 9).

### 3.2 Contact shape rendering in simulation

Given the geometric model of an object and its pose w.r.t. the sensor, we use rendering techniques to simulate contact shapes from object poses (Figure 1, bottom). We refer to this process as *geometric contact rendering*. Below, we describe how we compute contact poses, i.e., object poses w.r.t. the sensor that would result in contact without penetration; and their associated contact shapes:

1. We create a rendering environment using the open-source library Pyrender (*Pyrender n.d.*). In this environment, we place a virtual depth camera at the origin looking in the positive z-axis. The sensor can be then imagined as a flat surface (a rectangle in our case) orthogonal to the z-axis and at a positive distance  $d$  from the camera.
2. We place the object in any configuration (6D pose) such that all points in the object are at least at a distance  $d$  in the z-axis from the origin. We then compute the smallest translation in the z-axis that would make the object contact the surface that represents the sensor.
3. Finally, we move the object accordingly and render a depth image. The smallest pixel value of the depth image corresponds to a depth  $d$ , and we consider that only pixels between distances  $d$  and  $d + \Delta d$  are in contact with the sensor, where  $\Delta d$  represents the maximum deformation of the sensor. The rest are marked as non-contact. We convert the depth image to a binary image, where pixels with contact have a value of 1 and pixels with no contact have a value of 0. This binary image is the contact shape.

For our sensor, depth images have a width and height of 640x640 (later re-scaled to 160x160 for faster to compute), the distance to the origin is  $d = 10\text{mm}$ , and the maximum sensor deformation is  $\Delta d = 1.3\text{mm}$ .

### 3.3 Global tactile pose estimation

Once we know how to compute contact shapes both in simulation and from real tactile imprints, we reduce the problem of object pose estimation to finding what contact poses are more likely to produce a given contact shape. We solve this problem by first discretizing the space of possible contact poses as a parametrized grid, and then learning a similarity function that compares contact shapes.

**Object-dependent grids.** Using the 3D model of an object, we discretize the space of object poses in a multidimensional grid. Building a grid in the space of poses is a well-studied problem (Yershova et al. 2010; Roşca et al. 2014) that makes finding nearest neighbors trivial. It also allows each point on the grid to be seen as the representative of a volumetric part of the space which helps to reason over distributions. We prune the grid by only keeping object poses that result in contact, and then pair each of them with their respective

contact shape. Since we only consider poses that result in contact, this reduces the space of 6D poses to a 5D manifold. Using a grid, a discrete structured set of poses, allows us to easily account for object symmetries which can significantly reduce the grid size.

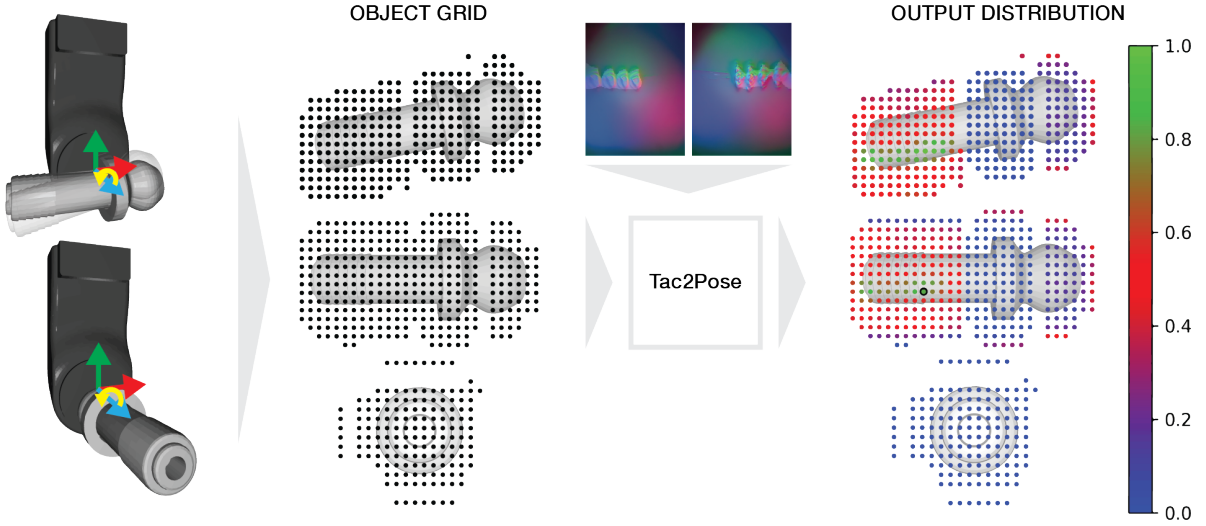
Our grids cover regions of the object which correspond to feasible grasp locations from the set of stable resting poses of the object on a surface. In particular, we include faces that correspond to feasible *grasp approach directions*, where the grasp approach direction specifies the axis of the grasp relative to the object. For some objects, we also include additional grasp approach directions that have interesting tactile features. For each grasp approach direction, We compute a dense set of contacts with 2.5mm translational resolution, and 6 degrees of rotational resolution around the axis of the grasp. As a result, the grid spans four coordinates (grasp approach direction,  $x$ ,  $y$ ,  $\theta$ ) and a contact pose will be no more than 1.25mm from an element of the grid, and often closer. A visualization of the grid dimensions can be seen in Figure 2. The number of elements in each grid varies between 3.8K and 181.3K, depending on the object size, shape, and number of grasp approach directions. We render each triplet of elements (two contacts, and the gripper opening) at 15 Hz, which can be parallelized. When grids are rendered serially, generating them takes from several minutes to many hours, depending on the grid size.

**Similarity metric for contact shapes.** Given a new contact shape, we compare it to all pre-computed contact shapes in the grid to find what poses are more likely to produce it. To that aim, we modify Momentum Contrast (MoCo) (He et al. 2019), a widely-used algorithm in contrastive learning, to encode contact shapes into a low dimensional embedding based on the distance between contact poses.

MoCo is able to learn unsupervised embeddings by building "a dynamic dictionary with a queue and a moving-averaged encoder". Instead, Tac2Pose is supervised and the elements in the queue are fixed and assigned to each of the poses in the object's grid. Given a new contact shape, our model learns to predict the likelihood that each pose in the grid has produced the given shape. This likelihood is computed by taking the softmax over the distances between the embedding of the new contact shape and the embeddings saved in the queue, which correspond to the embeddings of each contact shape in the grid. Compared to the original MoCo, Tac2Pose is supervised because during training, given a new contact shape, we can compute which element in the queue is closest to it.

To implement the encoder in our model, we use a ResNet-50 (He et al. 2016) cropped before the average-pooling layer to preserve spatial information, making it a fully-convolutional architecture. The loss function is the categorical cross-entropy loss which allows us to ensure that the output of the softmax is a well-defined probability distribution. The training data comes from selecting a random contact pose and finding its closest element in the dense grid. Then, we use as desired probabilities a vector of all zeros except for the closest element which gets assigned to probability one (see Figure 3). Section C in the Appendix contains further details on the learning method.

Once we have created a dense grid and trained a similarity encoder for an object, given a new contact shape at test time,



**Figure 2. Object grids.** The four dimensions of the grid with respect to the object are visualized (left): grasp approach direction, which is defined as the direction of the axis of the grasp (blue arrow), x translation (red arrow), y translation (green error), and angle in the plane of the grasp (yellow arrow). Samples of grid elements on the object long grease are shown as black dots, where each black dot represents the center location of the gripper during a grasp. Tac2Pose assigns likelihoods to each gripper location (right), given an observed contact (top). The most likely gripper locations for an observed contact are colored green, while the least likely are colored blue. The ground truth gripper location is shown as a black dot (right, center).

we can estimate which poses from the grid are more likely to generate it. To run Tac2Pose in real-time, we first encode the given contact shape and then compare it to all pre-computed encodings from the grid, which requires a single matrix-vector multiplication. Finally, we perform a softmax over the resulting vector of distances to obtain a probability distribution over the contact poses in the grid. We take the best match to be the contact pose with the highest probability, after (if applicable) incorporating additional pose constraints.

### 3.4 Multi-contact pose estimation

In this section, we show how to extend Tac2Pose to multi-contact settings where we simultaneously need to reason over several tactile observations. In Section D of the Appendix we show that the likelihood of an object pose from the grid,  $x$ , given the estimated contact shapes,  $C_{1,...,N}$ , from  $N$  sensors is proportional to

$$P(x|C_1, ..., C_N) \propto P(x|C_1) \cdot ... \cdot P(x|C_N) \cdot P(x) \quad (1)$$

where  $P(x)$  is a prior on the object pose, and the embedding network has been trained using uniformly-sampled poses.  $P(x|C_i)$  is the likelihood that pose  $x$  produces the contact shape  $C_i$  on sensor  $i$ . This allows combining Tac2Pose with additional pose constraints such as the ones coming from kinematics, previous tactile observations, or other perceptions systems.

The terms  $P(x|C_i)$  come directly from computing the similarity function between  $C_i$  and the contact shape from the grid of sensor  $i$  that is closest to the contact pose  $x$ . As a result, the computational cost of considering multiple contacts scales linearly with the number of sensors. In this paper, we consider the case of grasping with a parallel jaw gripper. We include information from two tactile images and the opening of the gripper during the grasp. We also consider the case of filtering the parallel jaw grasp distribution with a prior on the object pose.

## 4 Results

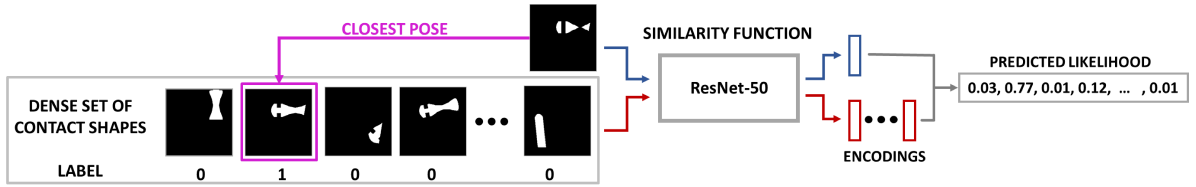
### 4.1 Real data collection

While Tac2Pose is trained purely with simulated data, in this section we describe how it can provide accurate pose estimation when evaluated on real tactile data. To that aim, we design a system that collects tactile observations on accurately-controlled poses. Below we describe the tactile sensor, the robot platform, and the objects used to perform the experiments.

**Tactile sensor.** We consider the tactile sensor GelSlim 3.0 (Taylor et al. 2021) which provides high-resolution tactile readings in the form of RGB images. The sensor consists of a membrane that deforms when contacted and a camera that records the deformation. The sensor publishes tactile observations through ROS as 470x470 compressed images at a frequency of 90Hz (see top left portion of Figure 1).

**Robot platform.** We collect labelled datasets of tactile observations of grasps on 20 objects mounted in known positions and orientations in the world. Each dataset contains pairs of RGB tactile images, and the corresponding ground-truth object pose relative to the gripper. The robotic system we use to collect the labelled datasets consists of a dual arm ABB Yumi with two WSG-32 grippers and GelSlim 3.0 tactile sensing fingers. We provide further details on the collection of labelled real data in Section B of the Appendix.

We collect labelled observations of feasible grasps on each object. We compute the contacts in each dataset by considering the *stable poses* of each object. Stable poses are the poses that an object is most likely to fall in when dropped onto a table. We then determine a set of feasible grasp approach directions for each stable pose. We define the grasp approach direction as the axis of the grasp during a parallel jaw grasp (Figure 2). For some objects, we also include additional grasp approach directions that have interesting tactile features. For each grasp approach direction, we collect



**Figure 3. Similarity function.** We build a similarity function that learns to encode contact shapes into a low dimensional space and predicts, given a new contact shape, the likelihood of being the closest match of each contact shape in the pre-computed set. By learning an encoder for the contact shapes, we can compare them very efficiently.

a set of equispaced real observations, that correspond to a given grasp approach direction at various x,y locations relative to the object. In total, these observations correspond to the set of contacts that we are likely to encounter when picking up each object from a table.

**Objects.** We test Tac2Pose on 20 objects, derived from CAD models of objects available on McMaster. During the selection of objects, we aimed at covering object features that differently impact tactile localization. The features we considered include:

1. *Contact non-uniqueness*: Contact non-uniqueness is the degree to which a contact is ambiguous, i.e., the contact in one pose resembles the contacts from other object poses (that are not equivalent under any symmetry). Non-unique contacts are more difficult to localize. An example of a non-unique contact on the object grease is shown in Figure 4 (second from right).
2. *Symmetry*: Object symmetries are sets of transformations under which the object pose is indistinguishable. Symmetry is a desirable property because it reduces the size of the grid.
3. *Object size*: Larger objects are generally more challenging to localize with tactile sensing alone, since a single touch corresponds to a more local view of the object.
4. *Contact size*: Large flat regions of contact with the sensor are generally more difficult to localize than smaller or textured ones. This is because most tactile sensors are less likely to produce crisp imprints for large flat contacts.

We share the CAD models of each of the objects we use on the project website.

## 4.2 Real pose estimation results

We evaluate the accuracy of Tac2Pose at estimating object poses from real tactile images. We note that Tac2Pose, even for large grids (100K elements), can easily run at 50Hz allowing real-time estimation of pose distributions. For each object, we evaluate Tac2Pose on 90 to 400 (varies depending on object size and number of grasp approach directions) pairs of real tactile images and object poses per object using the approach described in 4.1.

Given the ground truth object pose and our best estimate (the object pose with highest likelihood), we measure the resulting *pose error* (or distance between the two poses) by sampling a pointcloud of 10K points from the object

3D model and averaging the distance between these points when the object is at either of the two poses. This distance is sometimes called ADD (average 3D distance) but, for simplicity, we just refer to it as the pose error. To compare errors across shapes and object sizes, we also compute the *normalized pose error* which divides the original pose error by the average error obtained from predicting a random contact pose. Figure 4 shows examples of different normalized pose errors.

For each object, we evaluate the pose error for three ablations of Tac2Pose :

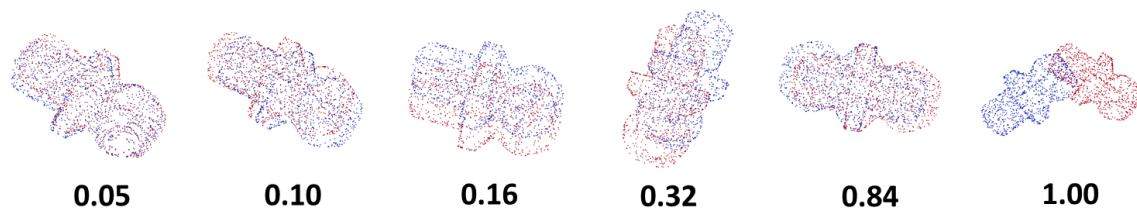
1. *Single Contact*: Estimate object pose from a single tactile image.
2. *Parallel Jaw*: Estimate object pose from a pair of tactile images, collected during a parallel jaw grasp on the object. The estimate also factors in the opening of the gripper during the grasp by computing the joint probability distribution of each object pose given both the two contacts and the gripper opening. In practice, this corresponds to multiplying the pose distribution obtained from the two contacts with a normal distribution centered around the gripper opening that each object pose would produce. The standard deviation of the normal distribution is 3mm which accounts for the expected error between the actual opening and the one reported by the gripper.
3. *Parallel Jaw + Prior*: Filter the distribution from the parallel jaw estimate to remove any poses that are more than a given pose distance from ground truth. This approximates cases in which an object pose is known within a margin of error, and is relevant when tactile localization is used to refine a coarse estimate of object pose from another sensing modality, like vision. We evaluate prior distances of 10mm and 5mm.

The median error for each ablation for each object is shown in Table 1.

We also aggregate the pose errors corresponding to the best estimate for each grasp, then visualize the distribution of errors as a violin plot in Figure 5, for selected objects. The medians reported in Table 1 correspond to the medians of the distributions visualized in the violin plots.

For each of the selected objects, we show three different error distributions, corresponding to the best estimates when using: a single contact (green distribution), parallel jaw contacts (blue distribution), and parallel jaw contacts plus a 10mm pose prior (purple distribution). To facilitate comparison between the objects, we plot normalized pose errors.





**Figure 4. Normalized pose errors**, i.e., pose errors w.r.t. to the average random error, for the object *grease*. The closest distance in the grid for this object is 0.03, similar to the first case. The median pose error when using parallel jaw contact information (0.10) corresponds to an error like the second case, and the average random error (1) would match with the last case. Finally, the example with 0.84 normalized error depicts a non-unique contact shape, i.e., the two object poses result in very similar contact shapes at the center that are not possible to distinguish without additional information.

Note that a normalized pose error of 1 corresponds to the expected error from selecting a pose at random from the grid. The **red** line measures the median pose error between the ground truth pose and its closest pose in the object’s grid of simulated contacts (a.k.a. the *closest error*). This sets a lower bound on the median performance for any given method.

**Single Contact.** We first analyze the performance of Tac2Pose with a single contact. Of the 20 objects we evaluate, 9 have median localization error with a single contact that is at least twice as good as random. These 9 objects have single contact normalized errors less than 0.5 in Table 1.

The objects that tend to perform best with a single contact are small objects with unique tactile features. For these objects, a single tactile imprint is often discriminative enough to fully determine the object pose. Consider the error distribution for *snap ring*, visualized in top row of Figure 5 as an example. Even with a single contact (**green** distribution), the error distribution has a clear primary mode which is centered near the closest error from the grid (**red** line). When incorporating additional constraints from a parallel jaw grasp, the distribution (**blue**) tightens around the closest error from the grid (**red** line), and secondary, higher error modes disappear. The median normalized error is approximately 0.10 for both the single contact and parallel jaw contact cases (Table 1). In other words, choosing the most likely pose using Tac2Pose results in, on average, approximately ten times less error than selecting a pose at random from the grid.

A sample contact that is localized within 1.3mm (0.09 normalized error) of the true pose using a single contact is visualized at left of the violin plot in Figure 5. This provides a sense of the scale of the errors.

**Parallel Jaw.** We next consider objects that perform significantly better with parallel jaw contacts. Of the 20 objects we evaluate, 11 have a median localization error with parallel jaw contacts that is more than twice as good as random. Of these 11 objects, 5 perform much better with parallel jaw contacts than with a single contact. The 5 objects satisfying both criteria are those in Table 1 where the parallel jaw normalized error is less than 0.5 and the single contact normalized error is more than double the parallel jaw contact normalized error. Two such objects are *long grease* and *hydraulic*.

The objects that perform significantly better with parallel jaw contacts compared with a single contact tend to be


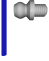
















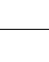

larger. Contacts with the object may appear as large, featureless patches from the local perspective of the tactile sensor. In general, large, flat contacts are more challenging to reconstruct from tactile images because they do not deform the gel membrane of the tactile sensor as much. Including the constraints of a second contact and the gripper opening provides higher robustness to noisy contact reconstructions. Furthermore, objects that vary significantly in width depending on where they are grasped benefit from parallel jaw contacts. In these cases, the additional constraint of the gripper opening during grasp can disambiguate between otherwise non-unique contacts. Recall that a contact is non-unique if its look similar to contacts where the object is in a different pose. In these cases, the contact is not a unique indicator of the object pose.

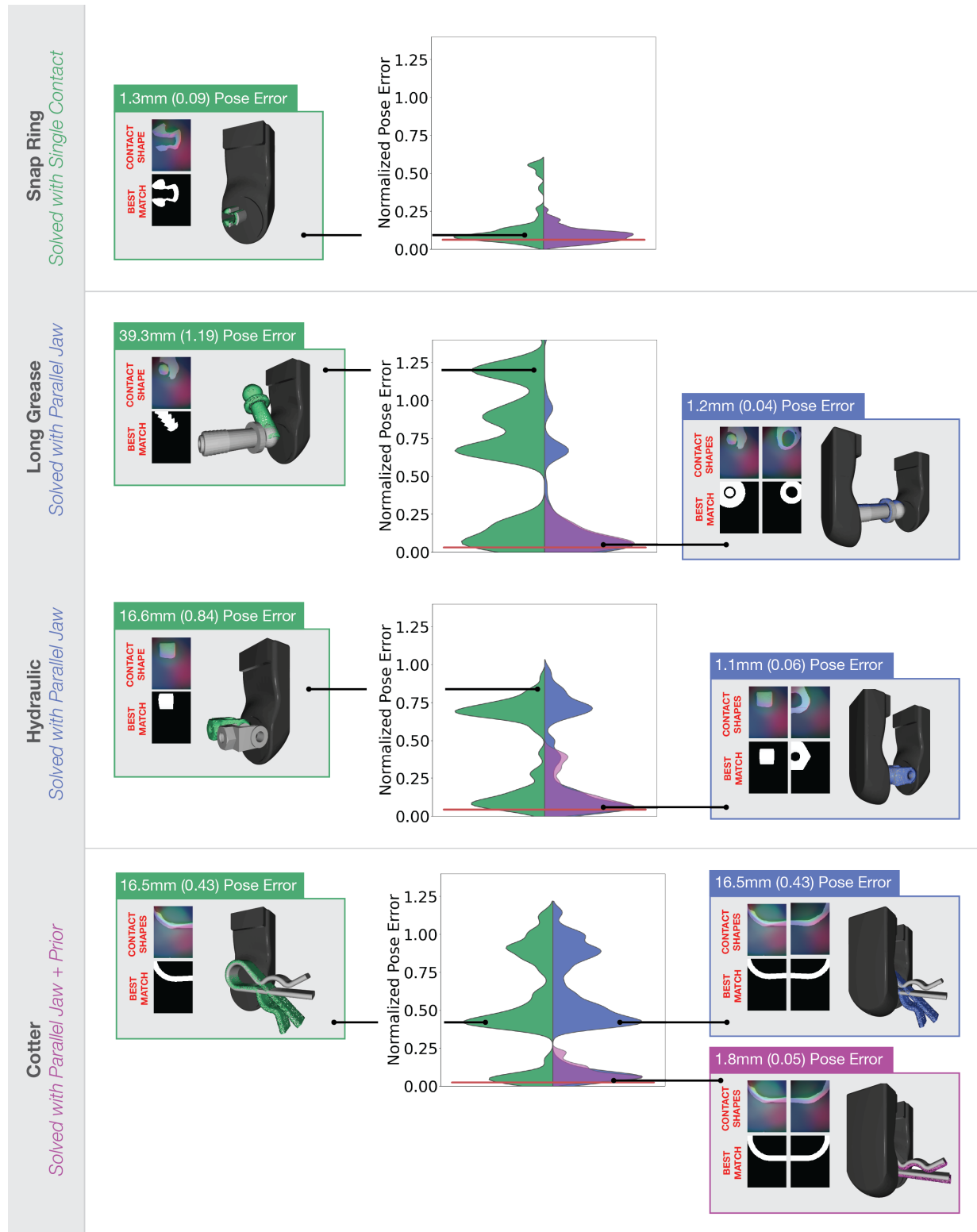
As an example, the error distribution for *long grease* is visualized as a violin plot in the second row of Figure 5. Considering parallel jaw information shifts the mode of the distribution much closer to the closest grid match (**red** line), and significantly reduces the prevalence of higher error modes. The medians of the error distributions for the single contact and parallel cases are significantly different; with a single contact, the median pose error is 26.6mm (0.76 normalized error) while with parallel jaw contacts, the median pose error is 3.3mm (0.10 normalized error). The random error, in comparison, is 35.2mm. With a single contact, Tac2Pose only performs about 1.3 times better than random. When including parallel jaw contacts, however, Tac2Pose is more 10 times better than random. The second row of Figure 5 (left of the violin plot) shows a sample contact on *long grease*, and the corresponding best match when using only a single contact (**green** pointcloud). The best match using a single contact is 39.3mm (1.19 normalized error) away from the true pose. The same contact, and the corresponding best match when using parallel jaw contacts (**blue** pointcloud) is visualized to the right of the violin plot. The best match using parallel jaw contacts is only 1.2mm (0.04 normalized error) away from the true pose. In this case, the additional information from the second contact and gripper opening is enough to resolve the ambiguity and substantially improve the localization.

Parallel jaw contacts can also be an important tool for disambiguating ambiguity inherent to the object geometry. As an example, consider a grasp on the object *hydraulic*, visualized at left of the violin plot in the third row of Figure 5. The true object pose is visualized as a grey mesh, whereas the best match using a single contact is visualized



**Table 1. Median error of the most likely pose.** We take the error corresponding to the most likely pose for each grasp on an object, and report the median. The blue line next to each object is 20mm long, to show relative object scale. We consider the error when using a single contact, parallel jaw contacts, and parallel jaw contacts + a pose prior (prior distances of 10mm and 5mm). We report the median error in mm, and as a normalized error (in parenthesis). To normalize the distributions filtered with a prior, we use the expected random error from the filtered distribution. Objects that can be localized accurately (more than twice as good as random) with a single contact are colored in green, objects that can be localized accurately after inclusion of parallel jaw information are colored in blue, and objects that can be localized accurately after inclusion of parallel jaw information and a 10mm prior on the object pose are colored in purple. Median values referenced in the text are bolded.

		Tactile Only		Pose Prior	
		Single Contact mm (norm)	Parallel Jaw mm (norm)	10mm Prior mm (norm)	5mm Prior mm (norm)
Snap Ring		<b>1.5 (0.10)</b>	1.4 (0.10)	1.4 (0.17)	1.4 (0.38)
Grease		1.3 (0.12)	1.2 (0.10)	1.2 (0.15)	0.9 (0.26)
Slotted Shim		4.0 (0.15)	3.0 (0.12)	2.4 (0.30)	2.3 (0.57)
Round Clip		3.4 (0.17)	11.5 (0.58)	2.0 (0.24)	1.9 (0.50)
Hanger		6.6 (0.19)	2.6 (0.07)	2.4 (0.30)	2.4 (0.57)
Pin		6.5 (0.20)	5.6 (0.17)	4.7 (0.66)	3.6 (1.02)
Big Head		7.8 (0.20)	6.1 (0.16)	4.9 (0.72)	3.9 (1.19)
Holder		5.8 (0.26)	2.2 (0.10)	1.8 (0.23)	1.8 (0.45)
Round Couple		13.6 (0.53)	10.9 (0.43)	6.0 (0.75)	3.5 (0.91)
Hydraulic		14.0 (0.67)	<b>4.9 (0.23)</b>	2.5 (0.31)	2.0 (0.49)
Long Grease		26.6 (0.76)	<b>3.3 (0.09)</b>	2.3 (0.33)	2.3 (0.61)
Stud		33.7 (0.85)	13.4 (0.34)	4.8 (0.57)	3.4 (0.82)
Cotter		19.0 (0.49)	19.6 (0.51)	<b>2.9 (0.38)</b>	2.7 (0.70)
Cable Clip		10.2 (0.59)	11.7 (0.67)	2.5 (0.30)	1.9 (0.45)
Hook		24.5 (0.77)	27.2 (0.85)	3.0 (0.38)	2.4 (0.63)
Couple		20.7 (0.79)	19.9 (0.76)	3.5 (0.42)	2.6 (0.66)
Hose		39.0 (0.62)	41.6 (0.66)	7.8 (1.00)	4.2 (1.03)
Pencil		38.1 (0.69)	41.6 (0.76)	5.0 (0.62)	3.9 (1.05)
Round Hose		37.6 (0.70)	37.3 (0.69)	5.5 (0.71)	4.2 (1.05)
Long Pencil		77.5 (0.96)	78.5 (0.97)	6.9 (0.85)	4.3 (1.01)



**Figure 5.** Error distributions for snap ring (top row), long grease (second row), hydraulic (third row), and cotter (bottom row). Each violin plot contains three distributions. At left, the single contact error distribution is visualized in green. At right, the parallel jaw contact distribution is visualized in blue, while the parallel jaw distribution filtered with a 10mm prior is overlaid in transparent purple. The median closest grid error is visualized as a red line. This corresponds to the best possible median performance. The median random error corresponds to a normalized pose error of 1. To the left and right of each violin plot, we show the localization errors for a sample grasp on each object. In the green boxes, the true object pose (grey mesh) is visualized with the best match when using a single contact (green pointcloud). The blue boxes and purple box show the same true object pose (grey mesh) with the best match when using parallel jaw contacts (blue pointcloud), and parallel jaw contacts + a 10mm pose prior (purple pointcloud), respectively. A single contact is enough to, on average, localize snap ring accurately using Tac2Pose (top row). Parallel jaw contacts are enough to localize long grease and hydraulic accurately (second and third rows), even though a single contact is not. Parallel jaw contacts and a coarse (10mm) pose prior are enough to localize cotter accurately (bottom row), even though single contact and parallel jaw contact information are not enough.

as a **green** pointcloud. The localization error with a single contact, in this case, is 16.6mm (0.84 normalized error). When considering only contacts from one of the fingers, the contact shapes corresponding to the true object pose and the best match are indistinguishable. Considering parallel jaw contacts, on the other hand, resolves the ambiguity.

The same contact, and the corresponding best match using parallel jaw contacts, is visualized at the right of the violin plot in the third row of the same figure. The localization (**blue** pointcloud) using parallel jaw contacts is much better because the contact on the second finger provides critical information about the object’s pose. The localization improves from 16.6mm (0.84 normalized) error with a single contact, to 1.1mm (0.06 normalized) error with parallel jaw contacts.

All grasps on *hydraulic* in contact with this non-unique feature are subject to the same problem when considering information from only a single contact, and therefore the non-uniqueness impacts the overall localization quality; the median localization error for *hydraulic* with a single contact is 14mm (0.67 normalized error), while with parallel jaw contact is 4.9mm (0.23 normalized error). The violin plot in the third row of Figure 5 shows that the distribution of errors when using a single contact (**green**) is bimodal, with a portion of the second, high error, mode corresponding to flipped localizations, like the one shown at left of the violin plot. When considering the distribution of best match errors using parallel jaw contacts (**blue** distribution), we see that the density of the high error mode corresponding to the flipped localization decreases, and more probability mass shifts into the low error mode centered around the closest error.

In the case of *hydraulic*, it is informative to break out the results by *grasp approach direction*. The primary reason that the localization error with parallel jaw contacts is, on average, nearly 3 times better than with a single contact is that including parallel jaw contacts resolves the aforementioned non-uniqueness, which only impacts one of the two grasp approach directions. For the grasp approach direction that contains the non-unique feature, including parallel jaw contacts reduces the localization error by nearly 8 times. For the other grasp approach direction, including parallel jaw contacts reduces the localization error by 1.6 times.

Only one object, *round clip*, has significantly higher median error in the parallel jaw case (see Appendix for details) compared with the single contact case.

**Parallel Jaw + Prior.** Finally, we consider the performance of Tac2Pose with parallel jaw contacts plus a prior on the object pose. Pose priors, in practice, can be obtained using additional sensing modalities (e.g. vision), kinematics, or previous estimates of the object’s pose. Because tactile sensing is inherently local, an object can have non-unique contacts which won’t be possible to fully disambiguate even with parallel jaw contacts. In such cases, a prior on the object’s pose can help resolve these ambiguities. To test the effect of a prior on Tac2Pose, we take the prediction distribution over possible object poses, and filter any pose that is more than a given distance from ground truth. Note that this implementation of a pose prior requires knowledge of the ground truth object pose, but it is a useful proxy for cases in which the object pose is known roughly, but not accurately. We evaluate localization accuracy for prior

distances of 10mm and 5mm. Results for both prior distances for each of the 20 objects are listed in Table 1.

The objects that benefit most from incorporating a prior on the object pose are those with *discrete non-uniqueness*. An object with discrete non-uniqueness has features that are unique (i.e. create discriminate tactile imprints) relative to most other possible contacts on the object, with a discrete number of exceptions. This type of discrete non-uniqueness can be an inherent feature of the object, or an artifact of noisy and incomplete contact shapes. Because there is a discrete number of possible object poses that are likely to produce such a contact shape, we expect the distribution over object poses to have a discrete number of modes where the majority of probability mass is concentrated. In these cases, incorporating a pose prior can truncate the distribution in such a way that only one of the modes is left. In other words, because there is a discrete number of possible poses that are likely to produce a given contact, if we eliminate the higher error options using a pose prior, we are likely to get a near perfect match. Therefore, for some objects, even a coarse prior on the object pose results in precise localization when combined with tactile information.

We evaluate which objects benefit most from incorporating a pose prior by comparing the pose error of the best match after filtering the pose distribution, with the expected error from selecting a pose at random from the filtered distribution. The normalized error we report in Table 1 for the 10mm and 5mm prior ablations uses the expected random error from the filtered distribution. For the remainder of this section, we consider just the case of a 10mm pose prior. For 12 of the 20 objects we evaluate, using Tac2Pose on top of a 10mm pose prior results in performance more than twice as good as selecting a pose at random from the filtered distribution. For 5 of the 12 objects, incorporating a pose prior plays an important role in driving down the localization error. With just parallel jaw contact information, the median localization error for these 5 objects is not significantly better than selecting a pose at random from the grid (where here we take *significantly better* to be more than twice as good as random). However, after filtering the distribution with a 10mm prior on the object pose, Tac2Pose selects the best pose with more than twice as much accuracy as selecting a pose at random from the filtered distribution. The objects that benefit most from incorporation of a pose prior are those in Table 1 with parallel jaw normalized error greater than 0.5, but 10mm prior normalized errors less than 0.5. An example of an object for which the incorporation of a 10mm prior leads to significantly better localization is *cotter*.

By examining the multi-modal error distributions with a single contact, or parallel jaw contact (violin plot in the bottom section of Figure 5), we can notice that the object *cotter* is likely to benefit from using pose prior. Its error distributions have a discrete number of modes (three) where the majority of probability mass is concentrated. Note that the symmetry of *cotter* is such that parallel jaw contacts do not provide much new information relative to a single contact, so the distributions of error for a single contact and parallel jaw contacts are very similar. The median error is 19.0mm (0.49 normalized error) when using a single contact, and 19.6mm (0.51 normalized error) when using parallel jaw contacts. Incorporation of a 10mm prior on the object pose

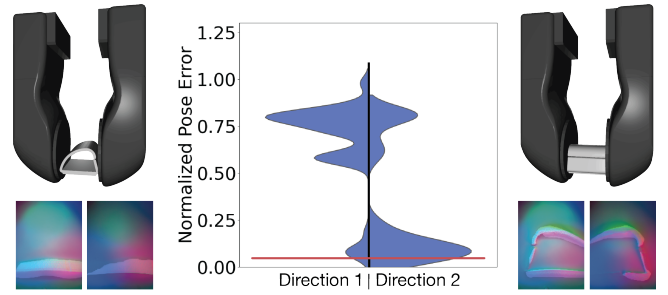
eliminates the two higher error modes, and shifts the median of the distribution toward the closest error. The median error becomes 2.9mm (0.38 normalized error), which is nearly seven times lower than using parallel jaw contact information alone. Recall that after incorporating a pose prior, the median error is normalized by the expected error from selecting a pose at random from the filtered distribution rather than from all contact poses.

We show an example of a grasp that benefits from a pose prior at left of the violin plots in the bottom row of Figure 5. With single or parallel jaw contacts, the localization error is 16.5mm (0.43 normalized). The contacts when cotter is in the given pose (grey mesh) are informative, but not completely unique relative to other possible contacts on the object. Incorporation of a coarse 10mm prior on the object pose, though, resolves the ambiguity, and the localization improves from 16.5mm (0.43 normalized) to 1.8mm (0.23 normalized) error for this grasp. The best match after filtering the parallel jaw distribution is visualized as a purple pointcloud on the right side of the violin plot in the bottom row of Figure 5.

**Comparing Grasp Approach Directions.** We evaluate multiple grasp approach directions for 13 of the 20 objects. For these objects, we compare the median localization error using parallel jaw contacts of each grasp approach directions. In practice, knowing which sets of grasps lead to lower localization errors could be leveraged in a grasp planning framework to select more informative grasps. There are 6 objects for which one direction has half as much error or less as the other(s): long grease, grease, hanger, hydraulic, round clip and round couple. Full results are shown in Table 6 in Appendix Section E. As example, we compare the two grasp approach directions for round clip in Figure 6. The first grasp approach direction, visualized in the left half of the figure, has non-unique contacts. As a result, the median normalized error is 15.2mm (0.85 normalized) when using parallel jaw contacts. The second grasp approach direction, visualized in the right half of the figure, has much more unique contacts; the median normalized error is 2.2mm (0.11 normalized), and the primary mode of the error distribution is concentrated near the closest grid error. The second grasp approach direction consists of grasps that, on average, lead to about eight times lower localization errors.

**Comparing Individual Grasps.** Some objects are difficult to localize even in the presence of a pose prior. For these objects, Tac2Pose does not reduce the median error much beyond the prior on the object pose. These objects are characterized by large, continuous, regions of non-unique contacts, and their error distributions tend to be broader, rather than having a discrete number of modes.

Long pencil (Figure 7a), for example, suffers from having large regions of non-unique contacts. Many of the contact poses along the length of the object result in the same information, and thus on average the match is chosen essentially at random from a large set of possible contacts. Note that this is not a limitation of Tac2Pose for tactile localization, but rather results from the object geometry and the local nature of tactile feedback; most contacts on long pencil are not sufficient to uniquely determine the object pose.

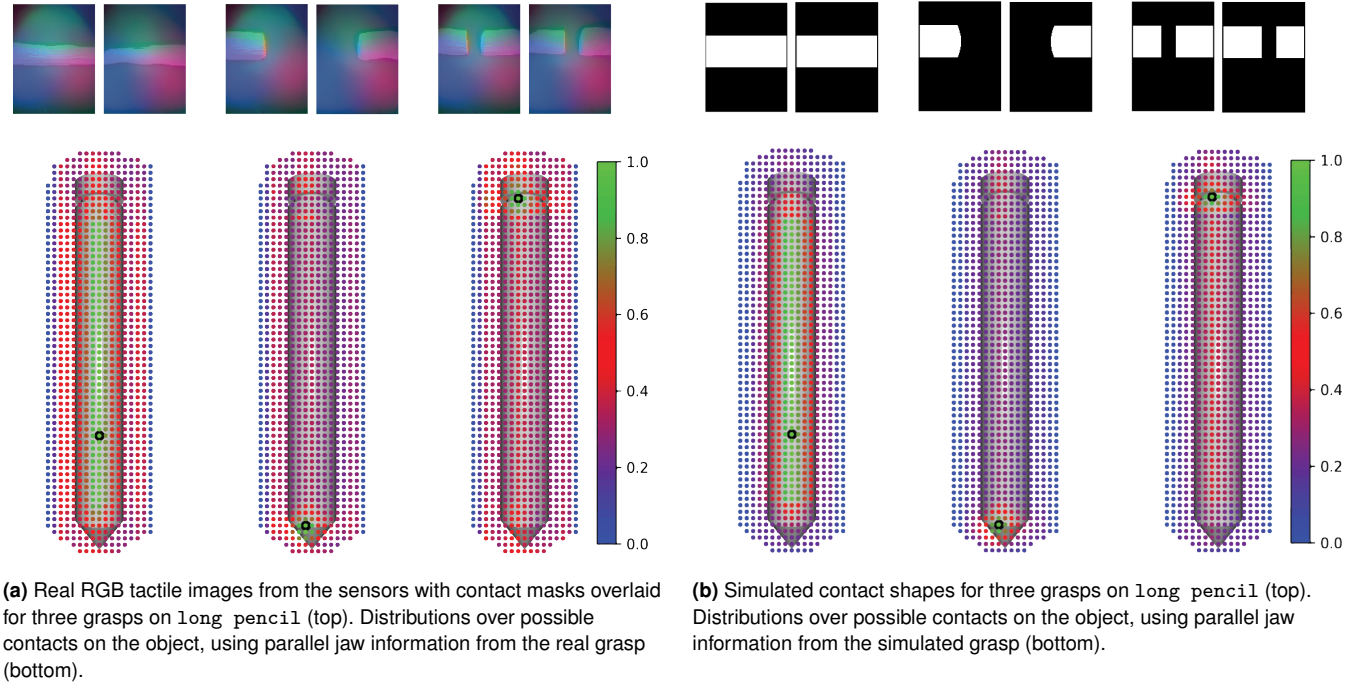


**Figure 6.** Error distributions for the first (left) and second (right) grasp approach directions on round clip using parallel jaw contacts. The red line represents the median closest grid error. The first grasp approach direction has more non-unique contacts (sample contacts visualized at left of the plot), and therefore has higher median error. Contacts in the second grasp approach direction, on the other hand, are much more unique (sample contacts visualized at right of the plot).

Even for objects with a large amount of non-uniqueness on average, there can be regions of the object which create distinctive and unique tactile imprints. Contacts near either end of long pencil, for example, are easier to localize accurately. Grasping on these regions leads to better localization. Depending on the downstream application, it might be beneficial to plan for grasps on an object that are expected to produce more unique tactile imprints, and thus lower localization errors. The existence of good grasps is something we can detect and exploit to avoid large regions of non-uniqueness, and achieve low localization errors. The distribution over contact poses for selected contacts on unique and non-unique regions of long pencil is shown in Figure 7a. The top row of the figure shows three possible grasps on the object. The bottom row shows the output of Tac2Pose - a distribution over possible contact poses. Each dot overlaid on long pencil represents a possible grasp location, and the color represents the likelihood that a given grasp generated the input tactile observation. The green dots are grasps with highest likelihood, while the blue dots are grasps with lowest likelihood. The black dot represents the true grasp location. Note that for ease of visualization, we show only points that represent center locations of the grasp when long pencil is oriented horizontally. This is a small subset (935) of the total number of contacts (65k) Tac2Pose reasons over. For contacts near the middle of the object (left of Figure 7a, for example), many grasps along the length of the object have high probability (green dots). For instance, the left contact in Figure 7a on its own is not enough to uniquely determine the object pose. In fact, the pose with the highest likelihood results in 77.9mm (0.99 normalized) error for this case. This aligns with our intuitive understanding that the best match is chosen essentially at random from a large set of likely contacts (green dots) along the middle of the object. Cases like this highlight the importance of outputting meaningful distributions over possible contact poses; the true contact pose has high likelihood, so Tac2Pose could be used in combination with information from other sensing modalities, kinematics, or previous tactile estimates to converge on a unique estimate of the true pose.

For contacts near the tips of the pencil (center and right of Figure 7a, for example), only grasps immediately





**Figure 7.** Output pose distributions for three grasps on long pencil, using real (7a) and simulated (7b) parallel jaw contacts. Each dot represents a possible grasp center location when the object is oriented parallel to the table, and its color represents the likelihood that a given grasp generated the tactile observation. The true grasp location is shown as a black dot. The left grasp in both sub-figures is on a non-unique region of the object; many grasps along the length of the object have high probability (green dots). On the other hand, the grasps at center and right of both sub-figures are on unique regions of the object. Only grasps immediately surrounding the true grasp (black dot) have high probability (green dots). The distributions from the real and simulated contact masks are qualitatively similar.

surrounding the correct tip have high probability. The cases illustrated result in 6mm (0.09 normalized) for the center contact, and 7mm (0.09 normalized) for the right.

In Figure 7b, we show distributions over contact poses for simulated versions of the same three contacts on long pencil. The output distributions when using simulated contacts are qualitatively similar as when using real contacts. Simulated contact shapes can therefore be used to detect regions of non-uniqueness before ever encountering the object. This feature could be used in a grasp planning framework to avoid regions of non-unique contacts and promote accurate, unique pose estimation from a single grasp.











### 4.3 Comparison with Scanned Object Models

Tac2Pose relies on apriori knowledge of the object geometry, in the form of a 3D CAD model. In Section 4.2, we evaluate Tac2Pose on manufacturer’s CAD models. Here, we consider the case where the object model is reconstructed using a 3D scanner. In particular, we use a SOL 3D Scanner by Scan Dimension, to generate the scanned object models.

We simulate a grid of possible object contacts and contact poses using the scanned object model. At test time, we compare contacts observed on the real object (same real datasets used in Section 4.2) against this imperfect set of simulated contacts.

We evaluate the accuracy of Tac2Pose when using scanned object models for 5 of the 20 objects, long grease, snap ring, big head, cotter, and hanger. We qualitatively compare the scanned and manufacturer’s CAD models for each of the 5 objects in Table 2. The left column shows the

**Table 2.** Pose error and normalized pose error (in parenthesis) for Tac2Pose on manufacturer’s CAD models versus scanned object models. We compare results with parallel jaw contacts + 10mm pose prior.

	Scanned Model mm (norm)		Manufacturer’s Model mm (norm)	
Snap Ring		1.6 (0.19)		1.4 (0.17)
Hanger		3.0 (0.39)		2.4 (0.30)
Long Grease		2.5 (0.33)		2.3 (0.33)
Cotter		4.0 (0.51)		2.9 (0.38)
Big Head		6.4 (0.88)		4.9 (0.72)

result of the 3D scan, and the right column shows the true object model.

When evaluating on the scanned object models, we relax the parameter that controls our confidence in the measurement of the gripper opening to reflect the fact that we expect the scanned object models to provide noisy information about the object geometry. The intuition for this decision is the following: when the object model is known, the gripper opening is a reliable signal of object pose. Therefore, we only want to assign high likelihood to those contact poses that match the observed gripper opening

closely. When the object model is reconstructed with a scanner, we cannot be as confident that the gripper opening we measure corresponds closely to the opening of the true nearest contact pose in the grid. This is because the gripper opening computed using the scanned model will be noisy. Therefore, we may want to assign high likelihood to a contact pose, even if the observed gripper opening does not match the opening of the contact pose as closely.

Table 2 compares the localization accuracy on scanned models versus manufacturer’s CAD models for the 5 objects, when using parallel jaw contact information with a 10mm pose prior. Although globally the geometry of the object looks similar between the scanned and manufacturer’s CAD models, there are clear differences at the local level. This ablation of Tac2Pose allows us to evaluate whether we are still able to achieve significant pose refinement, even when the local geometries are noisy.

We find that the error is comparable to that when using a manufacturer’s CAD model for all 5 objects. The normalized error is between 1.01 times (long grease) and 1.33 times (cotter) higher when using a scanned model compared with the manufacturer’s CAD model. Cotter is most impacted by using a scanned object model because the contact non-uniqueness becomes less discrete. When the object model is known exactly, many of the contacts look unique with a discrete number of exceptions. Therefore, even a coarse prior on the object pose leads to precise localization. When the object model is noisy, the discrete nature of the non-uniqueness is impacted for a fraction of the contacts, and the median localization error increases.

For snap ring, hanger, long grease, and cotter Tac2Pose is able to improve on the 10mm prior by a significant amount. For the first three objects, including parallel jaw information on top of the 10mm prior results in localization errors twice as low as selecting a pose at random from the filtered distribution (in Table 2, the normalized pose errors for the scanned objects are less than 0.5). For cotter, the localization error is nearly twice as low as selecting a pose at random from the filtered distribution (in Table 2, the normalized pose error is 0.51). For these four objects, Tac2Pose is able to refine the object pose within a small amount of error, even when local geometry is noisy. For big head, the amount of error is comparable (1.22 times higher) to that when using a manufacturer’s CAD model. Because big head has a symmetry-breaking feature around its principle axis, many contacts are continuously non-unique, and therefore the localization error does not improve much when incorporating a coarse prior, even when the object model is known.

#### 4.4 Comparison with Baselines

Next, we compare Tac2Pose to pose estimation from tactile images with three baseline methods:

1. *Pixel*: We perform direct pixel comparison between the observed contact mask, and each of the contact shapes in the grid.
  - 1.1. *Single Contact*: We select the grid shape that has the most pixels in common with the observed contact mask as the best match. We take the

object pose to be that corresponding to the best match in the grid.

- 1.2. *Parallel Jaw*: We take into account both tactile images and the gripper opening during a parallel jaw grasp. To do so, we compare the pair of observed contact masks, and the observed gripper opening, with triplets of contact masks and gripper openings from the grid. We sum the pixel error from each of the contacts, and the normalized error between the observed opening and the grid opening, to score each of the parallel jaw triplets in the grid. We take the object pose to be the contact pose corresponding to the triplet with the lowest score.
2. *Classification*: We formulate the task of pose prediction as a standard classification problem between the elements of the grid. We train a convolutional neural network (CNN) based on ResNet-50 to predict a distribution over the grid elements from a given contact mask. Recall that in Tac2Pose, the neural network is an encoder that maps contact shapes to vectors and we obtain a distribution over object poses by comparing the encoding from an observed contact shape to all the encodings from the contact shapes in the grid. In contrast, the neural network in the classification baseline learns to predict the distributions over object poses directly. We train this baseline by using the same data generation as in Tac2Pose. The inputs are simulated contacts that we obtained from slightly perturbing a pose from the grid and rendering its corresponding contact. For each of these new contacts, we compute its closest grid element and use as training label a vector with length equal to the number of elements as the grid, where all its values are zero except the entry corresponding to the index of the closest element, which has value one. This vector represents a probability distribution that measures the likelihood of each element of the grid to be the closest to the new contact. The loss function is the cross-entropy loss between the predicted likelihood and the classification label. At test time, from an observed tactile image in the form of a contact mask we obtain a distribution over grid elements.
3. *Pose*: We train a CNN based on ResNet-50 to regress a nine-element representation of the object pose based on an observed tactile image. The training data consists of contact shapes as inputs, and the contact poses that generated such contacts as labels. Each label is a pose represented by three translational elements, and six rotational elements that can be mapped into a rotation matrix. In comparison with quaternions, our 6D representation of rotations is continuous (meaning that similar orientations are close together in 6D representation), and therefore better suited to regression. We construct the last column of the rotation matrix from the 6D representation by applying Gram-Schmidt as a post-process on the first two columns, and taking the third column as the cross product of the first two (Zhou et al. 2018). The loss

function is the mean squared error between the output and true nine-element pose. This method for pose prediction does not rely on matching to elements on the grid, but rather predicts the pose of the object directly using supervised regression.

Both Tac2Pose and pixel are compatible with using parallel jaw information, while classification and pose only work with single contacts.

We evaluate the performance of Tac2Pose compared to baselines for 5 of the 20 objects: long grease, snap ring, big head, cotter, and hanger. We select these 5 objects to cover a range of difficulty in terms of grid size and degrees of symmetry and non-uniqueness.

### Baseline comparison with simulated data.

We first evaluate each method on sets of 100 simulated contacts per object. We sample 100 contact poses from the object's grid, add noise to each pose, and render the contacts corresponding to the new poses.

For each of the 5 baseline objects, we create three smaller, simpler, grids in addition to the original. The reduced grids serve to test each method's ability to scale to different problem sizes and types of complexity.

Recall that the original grids are determined by 4 spatial coordinates (grasp approach direction,  $x$ ,  $y$ ,  $\theta$ ) as illustrated in Figure 2. They have angular resolution of 6 degrees, and  $x$ ,  $y$  translational resolution of 2.5mm. The size of the original grids for the baseline objects ranges from 8.1k to 91.5k poses. The reduced grids are modified as follows:

1. *Mini One Face*: We include only one grasp approach direction, and one angle. We consider translations in  $x$ ,  $y$  with 5mm resolution. This grid is much smaller than the original (ranging from 29 to 124 poses, depending on the object), and is effectively 2D ( $x$ ,  $y$ ).
2. *Bigger Mini One Face*: We include only one grasp approach direction, and 10 angles (angular resolution of 36 degrees). We consider translations in  $x$ ,  $y$  with 5mm resolution. This grid is smaller than the original, and ranges from 331 to 1137 poses, depending on the object. It is effectively 3D ( $x$ ,  $y$ ,  $\theta$ ).
3. *One Face*: We include only one grasp approach direction, with full angular (6 degrees) and translational (2.5mm) resolution. This grid ranges in size from 4.8k to 26.8k poses, depending on the object. It is effectively 3D ( $x$ ,  $y$ ,  $\theta$ ). For snap ring, which only has one grasp approach direction even in the full sized grid, this grid is equivalent to the original and is therefore omitted.

Comparing results between the reduced grids can provide insight into each method's sensitivity to problem size, resolution, and complexity. For example, comparing mini one face and one face can indicate the sensitivity of each method to grid size and resolution. Comparing one face and the original grid (called full from here on out), which have the same resolution but cover different faces, provides insight into how each method handles complexity in the form of 3D rotations. Mini one face and bigger mini one face have the same translational resolution, but bigger

mini one face varies the angle in the plane of the grasp. Comparing results on these two grids provides insight into how incorporating rotations in the plane of the grasp impacts the accuracy of each method.

We first conduct experiments using only simulated data. The full set of results on the 5 baseline objects are listed in Table 3. We consider the results for hanger, visualized in Figure 8a, for simulated contacts from mini one face, bigger mini one face, one face, and full. The trends we note for this object are representative of the trends for the remaining objects.






The performance of classification (green bar) is inversely correlated with grid size; its performance is comparable to Tac2Pose only for mini one face (MOF in Figure 8a), which has 124 contacts. The normalized error is 0.12, compared with 0.08 for the single contact case of Tac2Pose. This indicates that although classification could be effective for very small grid sizes, the grids quickly become too large. Even with bigger mini one face, which contains 794 transformations, classification has a normalized error of 0.6, making it more than six times worse than Tac2Pose (single contact), which has 0.09 normalized error.

The classification baseline struggles with larger grid sizes because it needs to provide a classification over all elements in the grid, which often contains thousands of elements (the full grid for hanger, for example, has more than 90k contact poses). In comparison with the classification baseline, Tac2Pose scales better to large grid sizes because it learns to generate an embedding space based on the distance between contact poses. The encoder in Tac2Pose learns to push distant contacts away in embedding space, and therefore when comparing a new encoding to all the encodings in the grid, this direct comparison scales better than classification when the set of contacts in the grid is large. Instead, in classification the learned NN needs to encapsulate all the information relevant about all poses solely in the NN weights. Another way to think about the difference is to consider Tac2Pose as describing each contact in the grid with 1000 parameters (the encoder), whereas with classification, each contact in the grid is described by a single parameter (0 or 1).

The pose baseline (purple bar), on the other hand, is most comparable to Tac2Pose for the larger grids with high resolution. For one face (OF in Figure 8a), which covers one object face with the same translational and rotational resolution as the full grid, the normalized pose error using pose is 0.26, compared with 0.04 for the single contact version of Tac2Pose. For the full grid, the normalized error for pose and the single contact version of Tac2Pose is 0.18 and 0.08, respectively. In the absence of contact shape noise (simulated contacts), Tac2Pose is about 2.3 times better on the full grid. Recall that the pose baseline does not match observed contacts to contact poses on the grid, but instead regresses the corresponding contact pose directly. In pose, the learned NN needs to encapsulate all information relevant about all poses solely in the NN weights, as it doesn't have access to embeddings it can compare against.

The pixel baseline, for both single contact and parallel jaw contact cases, performs most comparably to Tac2Pose for the mini one face grid. The mini one face grid

**Table 3.** Pose error and normalized pose error (in parenthesis) for Tac2Pose versus baseline methods for a range of grid sizes, using 100 randomly simulated contacts per grid. Columns labelled SC are evaluated with a single contact, while columns labelled PJ use parallel jaw information.

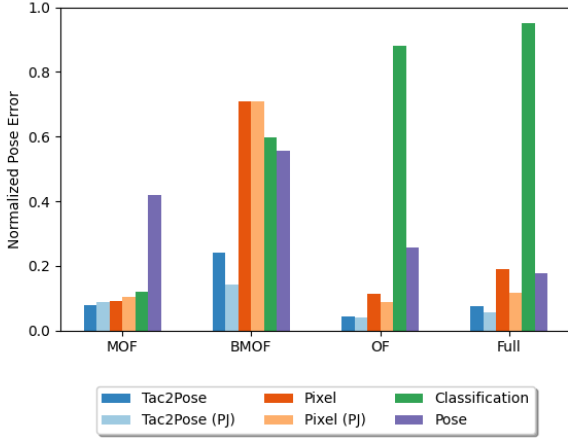
	Tac2Pose		Pixel		Classification	Pose
	SC mm (norm)	PJ mm (norm)	SC mm (norm)	PJ mm (norm)	SC mm (norm)	SC mm (norm)
<b>Long Grease</b> 						
Mini One Face	2.3 (0.09)	2.3 (0.09)	2.7 (0.11)	2.4 (0.09)	2.1 (0.08)	16.1 (0.57)
Bigger Mini One Face	18.1 (0.51)	11.5 (0.31)	27.1 (0.76)	16.6 (0.45)	34.8 (0.99)	25.2 (0.71)
One Face	1.5 (0.04)	1.3 (0.04)	12.0 (0.35)	4.8 (0.14)	32.7 (0.96)	7.5 (0.22)
Full	1.3 (0.04)	1.3 (0.04)	5.0 (0.14)	2.2 (0.06)	33.8 (0.92)	21.6 (0.59)
<b>Snap Ring</b> 						
Mini One Face	2.0 (0.16)	2.0 (0.16)	2.1 (0.14)	2.1 (0.15)	1.2 (0.11)	8.5 (0.76)
Bigger Mini One Face	3.1 (0.20)	3.1 (0.22)	6.9 (0.44)	6.9 (0.45)	2.6 (0.16)	10.1 (0.63)
Full	1.0 (0.06)	1.0 (0.07)	1.2 (0.08)	1.2 (0.08)	7.2 (0.49)	4.9 (0.33)
<b>Big Head</b> 						
Mini One Face	2.5 (0.09)	2.3 (0.09)	3.5 (0.13)	3.2 (0.12)	13.4 (0.50)	21.5 (0.81)
Bigger Mini One Face	37.5 (0.83)	14.6 (0.34)	37.9 (0.89)	31.1 (0.77)	43.4 (1.04)	30.5 (0.73)
One Face	1.7 (0.05)	1.6 (0.05)	4.8 (0.15)	4.7 (0.14)	31.4 (0.97)	15.6 (0.48)
Full	1.6 (0.04)	1.6 (0.04)	9.9 (0.23)	9.9 (0.23)	39.6 (0.97)	13.8 (0.34)
<b>Cotter</b> 						
Mini One Face	2.5 (0.08)	2.5 (0.10)	15.5 (0.52)	17.7 (0.60)	2.1 (0.07)	19.6 (0.71)
Bigger Mini One Face	8.3 (0.21)	8.8 (0.21)	34.0 (0.87)	34.0 (0.87)	15.2 (0.39)	22.2 (0.56)
One Face	1.3 (0.03)	1.4 (0.03)	5.8 (0.15)	6.2 (0.16)	35.2 (0.90)	8.5 (0.22)
Full	13.8 (0.34)	8.9 (0.22)	17.1 (0.44)	18.2 (0.42)	34.9 (0.88)	18.2 (0.46)
<b>Hanger</b> 						
Mini One Face	2.3 (0.08)	2.2 (0.09)	2.5 (0.09)	2.6 (0.10)	2.8 (0.12)	9.8 (0.42)
Bigger Mini One Face	9.1 (0.24)	5.1 (0.14)	25.2 (0.71)	25.1 (0.71)	21.1 (0.60)	19.6 (0.56)
One Face	1.5 (0.04)	1.4 (0.04)	4.0 (0.11)	3.3 (0.09)	30.9 (0.88)	9.0 (0.26)
Full	2.6 (0.08)	1.9 (0.06)	6.6 (0.19)	4.2 (0.12)	34.2 (0.95)	6.4 (0.18)

is small and simple enough (one angle, one face) that all methods (excluding pose) perform comparably. For one face and full, Tac2Pose outperforms pixel by about 2-3 times for both single contact and parallel jaw cases, which is still relatively comparable. This implies that pixel is most successful for high resolution grids. The performance of the pixel baseline method degrades most when the grid is low resolution, particularly when the grid contains object rotations. Bigger mini one face (shown as BMOF in the figure) has 0.71 median normalized error, compared with 0.24 for Tac2Pose (single contact). With parallel jaw contacts, the pixel baseline has 0.71 median normalized error, compared with 0.14 for Tac2Pose. Tac2Pose outperforms pixel by nearly 3 times in the single

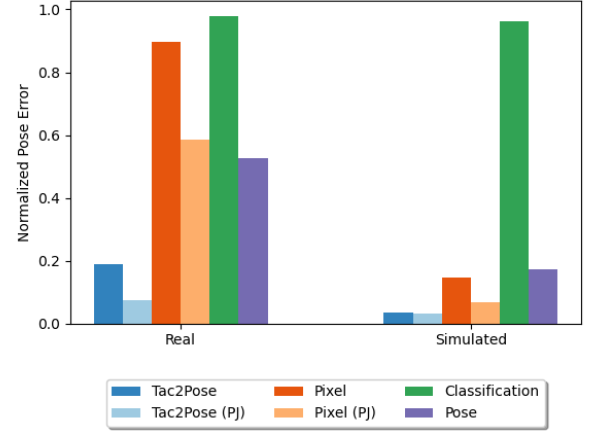
contact case, and more than 5 times in the parallel jaw case. Furthermore, pixel (both single contact and parallel jaw contact cases) is the least effective method when the grid is low resolution but complex.

When the grid resolution is low, the nearest grid match will be farther (in pixel distance) from an observed contact than when the grid resolution is high. This is particularly harmful for pixel when rotations are introduced, because a rotated version of a remote contact may, by chance, have more pixel overlap with the observed contact than the true closest match. This is much less likely to occur for high resolution grids, in which there exists a very close match on the grid to any observed contact. When the grid is simple (does not contain planar or 3D rotations) pixel can be successful even





(a) Results for 100 randomly sampled *simulated* contacts across four hanger grid sizes. Mini One Face (MOF) is the smallest and simplest grid, while Full is the largest and most complex.



(b) Results on the hanger dataset (Section 4.2) with over 100 contacts, using the full-sized grid for all methods. We evaluate all methods on the same *real* (left) and *simulated* (right) contact shapes.

**Figure 8.** Normalized pose error for the object hanger using tactile matching (Tac2Pose) and three baseline methods. We compare the performance of each method on simulated contacts from different grid sizes in (8a), and on real vs. simulated versions of the contacts in the hanger dataset (Section 4.2) in (8b).

when the grid resolution is low (as is the case for mini one face) because the best match on the grid is still likely to have the smallest pixel distance. If the grid is sufficiently complex, it must also be high resolution for pixel to be relatively successful (as is the case for one face and full). It is worth noting that a drawback of pixel, particularly with high resolution grids, is the execution time. In order to choose the best match, an observed contact is compared with contact shapes corresponding to every contact pose in the grid. Execution time is doubled when considering parallel jaw information, because two contacts are compared for each contact pose. Pixel is therefore the slowest method we evaluated by a significant margin. In practice, matching a contact to a high resolution grid in real-time using pixel is likely infeasible. Instead, Tac2Pose only compares low-dimensional embeddings resulting in at least an order of magnitude speed-up.

Finally, Tac2Pose performs consistently for both single and parallel jaw simulated contacts for all grid sizes for hanger. Tac2Pose also outperforms all baselines for all grid sizes. The parallel jaw case of Tac2Pose slightly outperforms the single contact case for all hanger grid sizes, except mini one face, in which the single contact case outperforms parallel jaw by 0.08 versus 0.09 normalized error. Tac2Pose (both single contact and parallel jaw) also performs slightly better for high resolution grids (one face and full).

#### Baseline comparison with real data.

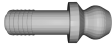




We next compare Tac2Pose against the three baselines, using the real datasets evaluated in Section 4.2 and full sized grids. The full set of results are listed in Table 4. We also evaluate simulated versions of the contacts in the real datasets, to assess each method’s sensitivity to noise in the contact shapes. The results on simulated versions of the contacts in the real datasets are listed in Table 5. We discuss in detail the results for hanger, visualized in Figure 8b. The trends for this object are representative of the trends we see overall.

For real data, and full-sized grids, the performance classification (green bar), and pixel with a single contact (dark orange bar) are similar to selecting a contact pose randomly from the grid. The median normalized error is 0.98 for classification, and 0.90 for pixel with a single contact. Pixel with parallel jaw contacts and pose perform better, and have errors almost two times lower than selecting a pose at random from the grid; the median normalized error is 0.59 for pixel with parallel jaw contacts, and 0.53 for pose. Tac2Pose (dark blue bar for single contact, light blue bar for parallel jaw contacts) significantly outperforms all baselines. The median normalized error for the single contact case is 0.19, and for the parallel jaw contact case is 0.07. Tac2Pose outperforms the next best baseline (pose) by nearly three times for the single contact case, and nearly eight times for the parallel jaw contact case.

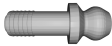




On simulated versions of the same contacts, pose and pixel (single contact and parallel jaw contact cases) both perform better than they do with real contacts. The median normalized error for pose shrinks by over three times, dropping to 0.17 with simulated data. Similarly, for pixel, the normalized error in simulation shrinks six times for single contact, and over eight times for parallel jaw contacts, dropping to 0.15 and 0.07, respectively. This indicates the sensitivity of both pose and pixel to noise in the contact shapes. Tac2Pose, in comparison, is more robust to contact shape noise, particularly in the parallel jaw contact case. With simulated contacts, the median normalized error for the parallel jaw case of Tac2Pose shrinks about two times, dropping to 0.03. Furthermore, despite the better performance of pose and pixel on simulated contacts compared with real contacts, Tac2Pose yields the best performance on simulated contacts as well. With simulated contacts, Tac2Pose is more than twice as good as the next best baseline (pixel with parallel jaw contacts).

The primary reason for pixel’s sensitivity to noise in the contact shapes is that it only evaluates the exact 2D location

**Table 4.** Pose error and normalized pose error (in parenthesis) for Tac2Pose versus baseline methods, on *real* datasets. Columns labelled SC are evaluated with a single contact, while columns labelled PJ use parallel jaw information.

		Tac2Pose		Pixel		Classification	Pose
		SC	PJ	SC	PJ	SC	SC
		mm (norm)	mm (norm)	mm (norm)	mm (norm)	mm (norm)	mm (norm)
Long Grease		26.6 (0.76)	3.3 (0.09)	32.8 (0.93)	6.0 (0.17)	33.3 (0.95)	25.3 (0.72)
Snap Ring		1.5 (0.10)	1.4 (0.10)	5.6 (0.39)	2.2 (0.15)	6.0 (0.42)	5.9 (0.41)
Big Head		7.8 (0.20)	6.1 (0.16)	27.6 (0.70)	11.7 (0.30)	35.0 (0.89)	33.8 (0.86)
Cotter		19.0 (0.49)	19.6 (0.51)	31.5 (0.81)	36.7 (0.95)	35.8 (0.93)	38.1 (0.99)
Hanger		6.6 (0.19)	2.6 (0.07)	31.3 (0.90)	20.5 (0.59)	34.2 (0.98)	18.3 (0.53)

**Table 5.** Pose error and normalized pose error (in parenthesis) for Tac2Pose versus baseline methods, on *simulated* versions of the real contacts used in Table 4. Columns labelled SC are evaluated with a single contact, while columns labelled PJ use parallel jaw information.

		Tac2Pose		Pixel		Classification	Pose
		SC	PJ	SC	PJ	SC	SC
		mm (norm)	mm (norm)	mm (norm)	mm (norm)	mm (norm)	mm (norm)
Long Grease		1.1 (0.03)	1.1 (0.03)	1.8 (0.05)	1.7 (0.05)	33.0 (0.94)	17.0 (0.48)
Snap Ring		1.0 (0.07)	1.0 (0.07)	1.2 (0.08)	1.2 (0.08)	6.0 (0.41)	4.5 (0.31)
Big Head		3.9 (0.10)	3.3 (0.08)	8.7 (0.22)	9.6 (0.24)	34.0 (0.87)	13.8 (0.35)
Cotter		1.3 (0.03)	1.3 (0.03)	17.9 (0.46)	17.7 (0.46)	35.0 (0.91)	13.2 (0.34)
Hanger		1.2 (0.03)	1.2 (0.03)	5.1 (0.15)	2.4 (0.07)	33.6 (0.96)	6.0 (0.17)

of the contact on the sensor. Tac2Pose, in comparison, is trained to match contact shapes resulting from slight perturbations of grid poses to the closest match on the grid. This makes Tac2Pose more robust to slight discrepancies between observed and grid contact shapes.

The sensitivity of pose to contact shape noise has to do, instead, with the method's ability to generalize to out of distribution data in the form of real contact shapes. Both pose and Tac2Pose are trained on simulated versions of contact shapes, but Tac2Pose generalizes to real contact shapes much better. Tac2Pose computes the likelihood of an observed contact matching to a discrete set of simulated shapes. Therefore, the match does not need to be exact, just better than other possible options, for the localization to be accurate. The structure imposed by the grid therefore improves the ability of Tac2Pose to generalize to real, noisy contact shapes. Because pose regresses object poses directly, without the structure of the grid, its performance is more brittle and degrades when using real contacts.

The normalized error of classification, even with simulated contacts, is 0.96, remaining similar to selecting a pose randomly from the grid. The size of the grid is too large to be handled with classification (as addressed in Section 4.4), so it is not possible to comment on the impact of noisy contacts.

For the 5 objects we evaluate (long grease, snap ring, big head, hanger, and cotter), Tac2Pose performs significantly better than random (here, we define significantly better as more than twice as good, which can be identified as a median normalized error less than 0.5 in Table 4) for 4/5 objects in both the single contact and parallel jaw contact cases. In the parallel jaw contact case, the fifth object, cotter, has median normalized error of 0.51, which is just below twice as a good as random. In comparison, pose, classification, and pixel with a single contact are only significantly better than random for 1/5 objects. Pixel with parallel jaw contacts is significantly better than random for 3/5 objects. Furthermore, with a single contact,

Tac2Pose outperforms all baselines for 4/5 objects. Tac2Pose is between 1.5 and 4 times better than the next best baseline for all objects except for long grease, which performs marginally worse than pose in the single contact case (0.72 median normalized error for pose, compared with 0.76 for Tac2Pose). With parallel jaw contacts, Tac2Pose outperforms pixel, which is the only other method compatible with parallel jaw contacts, with by between 1.5 and 9 times, depending on the object.

A final observation is that for some objects, parallel jaw contact versions of pixel and Tac2Pose are more robust to contact shape noise than single contact versions. We consider long grease (results listed in Table 4) as an example. Tac2Pose with a single real contact has 0.76 median normalized error, compared with 0.09 for the parallel jaw contact case. This means that the localization performance improves around eight times when using parallel jaw contacts. Similarly, pixel with a single contact has 0.93 median normalized error, compared with 0.17 median normalized error with parallel jaw contacts; the localization performance is about 5.5 times better in the parallel jaw contact case. We also consider the performance of Tac2Pose, and pixel, on simulated contacts to evaluate the impact of contact shape noise on the discrepancy between single and parallel jaw contact cases. With simulated contacts, the localization performance is the same for Tac2Pose for both a single contact and parallel jaw contacts; the median normalized error is 0.03 in both cases. The outcome is similar for pixel; the median normalized error is 0.05 in both the single contact and parallel jaw contact cases. The consistent localization performance between methods and contact configurations when using simulated contacts indicates that contact shape noise is the differentiating factor between single contact and parallel jaw contact cases when using real contacts. This means that robustness to noise is a key advantage of using parallel jaw contacts over a single contact, for both methods. Both Tac2Pose and pixel have similar performance in the parallel jaw case with real contacts as they do with idealized (simulated) contacts; it is 3 (Tac2Pose) to 3.5 (pixel) times easier to localize simulated contacts than real contacts. The discrepancy between simulated and real results is much more pronounced in the single contact case of both methods. This implies that the sim-to-real gap can be bridged, in part, by the inclusion of parallel jaw information.

We conclude this section with some remarks about the challenge of estimating an object’s pose from a single noisy contact. Tac2Pose outperforms all baselines on 4/5 objects with a single contact, and all objects with parallel jaw contacts. Ultimately, though, even Tac2Pose struggles to perform significantly better than selecting a pose at random from the grid with a single contact for 1/5 objects (where significantly better than random is defined as more than twice as good). Estimating the pose of an object from a single, noisy, often non-unique contact is challenging. Therefore, perhaps the most important feature of Tac2Pose is that it outputs meaningful pose distributions over possible object poses (Figure 7a). This creates a natural framework for incorporating constraints from additional contacts, measurements of the robot state (such as the gripper

opening), information from additional sensing modalities, or even previous tactile estimates of the object pose.

## 5 Discussion

This paper presents an approach to tactile pose estimation for objects with known geometry. Tac2Pose relies on learning an embedding completely in simulation that facilitates comparing real and simulated contact shapes. We can reconstruct contact shapes with high fidelity, using images from the real sensor and in simulation. We compare the embeddings of an observed contact shape with those of a precomputed dense set of simulated contact shapes to obtain the distribution over a dense set of possible object poses. The approach therefore allows to reason over pose distributions and to handle additional pose constraints.

We evaluate Tac2Pose on real grasp datasets for 20 objects, and report the accuracy for three ablations of Tac2Pose, corresponding to increasing amounts of information from a given grasp. First, we evaluate the accuracy using a single tactile image which corresponds to the case where only one contact is available to the algorithm. Second, we consider the case where two tactile images (corresponding to a parallel jaw grasp on the object) and the gripper opening are available. Third, we evaluate the accuracy after filtering the distribution obtained using parallel jaw information with a coarse prior on the object pose, approximating the case where information from an additional sensing modality (e.g. vision) is available.

We find that the amount of information needed to localize an arbitrary grasp on an object accurately is highly dependent on the object geometry. Of the 20 objects we evaluate, 9 can be localized accurately with a single contact. For these objects, more than half of arbitrary grasps on the object can be localized accurately. The objects that can be localized accurately with a single contact tend to be smaller, and have significant regions of unique contacts. When including parallel jaw information, the number of objects that can be localized accurately using the best match from Tac2Pose increases to 12. The objects that can be localized accurately after including parallel jaw information tend to have pseudosymmetrical features which can be disambiguated with a second contact, or vary significantly in width across the length of the object, which makes the gripper opening a discriminative source of information. After filtering the parallel jaw pose distribution with a coarse 10mm prior on the object pose, the number of objects that can be localized accurately increases to 16. The objects that can be localized accurately after including a coarse prior on the object pose tend to be larger, and have *discrete nonuniqueness* (features that are unique, with a discrete number of exceptions on remote regions of the object).

There are, however, four objects which cannot be localized accurately on average even after filtering the parallel jaw distribution with a 10mm prior and selecting the resulting most likely object pose. These objects are large, and have significant, continuous regions of non-unique contacts. The majority of contacts on such objects do not provide enough information to uniquely determine their pose.

Even objects which can be, on average, localized accurately from an arbitrary grasp have regions of non-unique contacts that do not provide enough information to uniquely determine the object pose. It is therefore important to evaluate the localization accuracy of specific grasps on objects, as well as arbitrary grasps. To this end, we compare the localization accuracy separated out by grasp approach direction, and the localization accuracy of individual grasps on selected objects. We find that many objects have one direction which is significantly easier to localize (half as much error or less) than others. By examining individual grasps on the object `long_pencil`, we find that even objects with large, continuous regions of non-unique contacts have regions that are more unique and easier to localize.

Both of these breakdowns (sets broken out by grasp approach direction, or individual grasps) could ultimately be leveraged in a grasp planning framework, in which grasps that are easier to localize are specifically targeted. In practice, grasps within a given grasp approach direction could be targeted with a very coarse prior on the object pose, while a specific individual grasp could be targeted with somewhat finer information about the object pose. Because Tac2Pose is trained entirely in simulation, it is possible to evaluate which grasps lead to lower localization error in advance of encountering the object. For instance, the output pose distributions we obtain using simulated and real contact shapes on `long_pencil` are qualitatively similar (Figure 7a and 7b). Simulated contacts can therefore be used to identify unique and non-unique candidate grasps. This feature, too, could be important to leverage in a manipulation planning framework.

Our approach also assumes we have access to accurate geometric models of objects. We demonstrate that Tac2Pose can be effectively combined with object models reconstructed from a 3D scanner. A key feature of Tac2Pose is the ability to refine coarse estimates of object pose with high resolution tactile information. We find that moderate shape noise does not significantly compromise that ability for any of the 5 objects we evaluate.

Future work could learn embeddings that are even more robust to shape uncertainty by corrupting the contact shapes with noise during training. This would not inherently improve the localization accuracy when considering only information from a single grasp, but could yield distributions that are more representative of our true confidence in the estimate. These distributions could be combined effectively with other information (e.g. pose priors, additional tactile measurements, or dynamics) to converge on a unique estimate of the object pose.

We demonstrate the advantages of Tac2Pose compared with baseline methods for estimating object pose from tactile images. Compared with a standard classification approach, direct pose regression, and direct pixel comparison, Tac2Pose scales better to larger, and more complex problems (e.g. regressing 6D object pose rather than simply translation or rotation in plane) and is more robust to contact shape noise.

In summary, we demonstrate the effectiveness of Tac2Pose at pose estimation for 20 objects with information gathered from a single, real grasp on the object. We consider known and reconstructed object shapes, and show that in both cases

Tac2Pose outputs meaningful distributions over object pose that can be maximized directly, or combined with additional information to converge on a unique estimate of object pose. While Tac2Pose is trained entirely in simulation, it is robust to real and noisy contact shapes arising from both sensor noise and object shape noise. This robustness stands in contrast baseline methods, which are more sensitive to contact shape noise. This suggests that matching estimated contact shapes to a dense precomputed set opens the door to moving many computations into simulation, without loss of robustness, and improving how robots learn to perceive and manipulate their environment.

## Acknowledgments

We thank Ian Taylor and Siyuan Dong for helping with the real setup. We also thank Ferran Alet for providing detailed insights and reviewing the paper.

## References

- Allen, P. K., Miller, A. T., Oh, P. Y. and Leibowitz, B. S. (1999), ‘Integration of vision, force and tactile sensing for grasping’, *Int. J. Intelligent Machines* **4**, 129–149.
- Bauza, M., Canal, O. and Rodriguez, A. (2019), Tactile mapping and localization from high-resolution tactile imprints, in ‘International Conference on Robotics and Automation (ICRA)’, IEEE.
- Bauza, M., Valls, E., Lim, B., Sechopoulos, T. and Rodriguez, A. (2020), ‘Tactile object pose estimation from the first touch with geometric contact rendering’, *CoRR* **abs/2012.05205**.  
**URL:** <https://arxiv.org/abs/2012.05205>
- Bimbo, J., Kormushev, P., Althoefer, K. and Liu, H. (2015), ‘Global estimation of an object’s pose using tactile sensing’, *Advanced Robotics* **29**(5), 363–374.
- Bimbo, J., Luo, S., Althoefer, K. and Liu, H. (2016), ‘In-hand object pose estimation using covariance-based tactile to geometry matching’, *IEEE Robotics and Automation Letters*.
- Chalon, M., Reinecke, J. and Pfanne, M. (2013), Online in-hand object localization, in ‘2013 IEEE/RSJ International Conference on Intelligent Robots and Systems’, IEEE, pp. 2977–2984.
- Chebatar, Y., Kroemer, O. and Peters, J. (2014), Learning robot tactile sensing for object manipulation, in ‘International Conference on Intelligent Robots and Systems’, IEEE.
- Corcoran, C. (2010), Tracking object pose and shape during robot manipulation based on tactile information, in ‘International Conference on Robotics and Automation (ICRA)’.
- Deng, X., Mousavian, A., Xiang, Y., Xia, F., Bretl, T. and Fox, D. (2019), ‘Poserbpf: A rao-blackwellized particle filter for 6d object pose tracking’, *CoRR* **abs/1905.09304**.  
**URL:** <http://arxiv.org/abs/1905.09304>
- Falco, P., Lu, S., Cirillo, A., Natale, C., Pirozzi, S. and Lee, D. (2017), Cross-modal visuo-tactile object recognition using robotic active exploration, in ‘Robotics and Automation (ICRA), 2017 IEEE International Conference on’, IEEE, pp. 5273–5280.
- Gao, W. and Tedrake, R. (2019), Filterreg: Robust and efficient probabilistic point-set registration using gaussian filter and twist parameterization, in ‘Proceedings of the IEEE



- Conference on Computer Vision and Pattern Recognition', pp. 11095–11104.
- He, K., Fan, H., Wu, Y., Xie, S. and Girshick, R. (2019), 'Momentum contrast for unsupervised visual representation learning', *arXiv preprint arXiv:1911.05722*.
- He, K., Zhang, X., Ren, S. and Sun, J. (2016), Deep residual learning for image recognition, in 'IEEE Conference on Computer Vision and Pattern Recognition (CVPR)'.
- Hogan, F. R., Bauzá, M., Canal, O., Donlon, E. and Rodriguez, A. (2018), 'Tactile regrasp: Grasp adjustments via simulated tactile transformations', *CoRR abs/1803.01940*.
- Ilonen, J., Bohg, J. and Kyrki, V. (2014), 'Three-dimensional object reconstruction of symmetric objects by fusing visual and tactile sensing', *The International Journal of Robotics Research*.
- Isola, P., Zhu, J.-Y., Zhou, T. and Efros, A. A. (2018), 'Image-to-image translation with conditional adversarial networks'.
- Izatt, G., Mirano, G., Adelson, E. and Tedrake, R. (2017), Tracking objects with point clouds from vision and touch, in 'International Conference on Robotics and Automation'.
- Javdani, S., Klingensmith, M., Bagnell, J. A., Pollard, N. S. and Srinivasa, S. S. (2013), Efficient touch based localization through submodularity, in 'International Conference on Robotics and Automation (ICRA)', IEEE.
- Jeon, M. and Kim, A. (2020), 'Prima6d: Rotational primitive reconstruction for enhanced and robust 6d pose estimation', *IEEE Robotics and Automation Letters* **PP**, 1–1.
- Kim, S. and Rodriguez, A. (2021), 'Active extrinsic contact sensing: Application to general peg-in-hole insertion'.
- Koval, M. C., Klingensmith, M., Srinivasa, S. S., Pollard, N. S. and Kaess, M. (2017), The manifold particle filter for state estimation on high-dimensional implicit manifolds, in '2017 IEEE International Conference on Robotics and Automation (ICRA)', pp. 4673–4680.
- Koval, M. C., Pollard, N. S. and Srinivasa, S. S. (2015), 'Pose estimation for planar contact manipulation with manifold particle filters', *The International Journal of Robotics Research*.
- Kuppuswamy, N., Castro, A., Phillips-Grafflin, C., Alspach, A. and Tedrake, R. (2019), 'Fast model-based contact patch and pose estimation for highly deformable dense-geometry tactile sensors', *IEEE Robotics and Automation Letters* **PP**, 1–1.
- Labbé, Y., Carpentier, J., Aubry, M. and Sivic, J. (2020), 'Cosypose: Consistent multi-view multi-object 6d pose estimation', *CoRR abs/2008.08465*.  
**URL:** <https://arxiv.org/abs/2008.08465>
- Lepora, N. F., Church, A., De Kerckhove, C., Hadsell, R. and Lloyd, J. (2019), 'From pixels to percepts: Highly robust edge perception and contour following using deep learning and an optical biomimetic tactile sensor', *IEEE Robotics and Automation Letters* **4**(2), 2101–2107.
- Li, R., Platt, R., Yuan, W., ten Pas, A., Roscup, N., Srinivasan, M. A. and Adelson, E. (2014), Localization and manipulation of small parts using gelsight tactile sensing, in 'Intelligent Robots and Systems (IROS), 2014 IEEE/RSJ International Conference on'.
- Li, Y., Wang, G., Ji, X., Xiang, Y. and Fox, D. (2018), 'Deepim: Deep iterative matching for 6d pose estimation', *CoRR abs/1804.00175*.  
**URL:** <http://arxiv.org/abs/1804.00175>
- Luo, S., Bimbo, J., Dahiya, R. and Liu, H. (2017), 'Robotic tactile perception of object properties: A review', *Mechatronics* **48**, 54–67.
- Luo, S., Mou, W., Althoefer, K. and Liu, H. (2017), 'Localizing the object contact through matching tactile features with visual map', *CoRR abs/1708.04441*.
- Milan, A., Pham, T., Vijay, K., Morrison, D., Tow, A. W., Liu, L., Erskine, J., Grinover, R., Gurman, A., Hunn, T., Kelly-Boxall, N., Lee, D., McTaggart, M., Rallos, G., Razjigaev, A., Rowntree, T., Shen, T., Smith, R., Wade-McCue, S., Zhuang, Z., Lehnert, C., Lin, G., Reid, I., Corke, P. and Leitner, J. (2018), Semantic segmentation from limited training data, in 'International Conference on Robotics and Automation (ICRA)', IEEE.
- Petrovskaya, A. and Khatib, O. (2011), 'Global localization of objects via touch', *IEEE Transactions on Robotics* **27**(3), 569–585.
- Pezzementi, Z., Reyda, C. and Hager, G. D. (2011), Object mapping, recognition, and localization from tactile geometry, in 'International Conference on Robotics and Automation (ICRA)'.
- Platt, R., Permenter, F. and Pfeiffer, J. (2011), 'Using bayesian filtering to localize flexible materials during manipulation', *IEEE Transactions on Robotics* **27**(3), 586–598.
- Pyrender (n.d.), <https://github.com/mmatl/pyrender>.
- Roşca, D., Morawiec, A. and De Graef, M. (2014), 'A new method of constructing a grid in the space of 3d rotations and its applications to texture analysis', *Modelling and Simulation in Materials Science and Engineering* **22**(7), 075013.
- Saund, B., Chen, S. and Simmons, R. (2017), Touch based localization of parts for high precision manufacturing, in 'International Conference on Robotics and Automation (ICRA)', IEEE.
- Schaeffer, M. A. and Okamura, A. M. (2003), Methods for intelligent localization and mapping during haptic exploration, in 'International Conference on Systems, Man and Cybernetics', IEEE.
- Schwarz, M., Lenz, C., García, G. M., Koo, S., Periyasamy, A. S., Schreiber, M. and Behnke, S. (2018), Fast object learning and dual-arm coordination for cluttered stowing, picking, and packing, in 'International Conference on Robotics and Automation (ICRA)', IEEE.
- Sodhi, P., Kaess, M., Mukadam, M. and Anderson, S. (2020), 'Learning tactile models for factor graph-based state estimation', *CoRR abs/2012.03768*.  
**URL:** <https://arxiv.org/abs/2012.03768>
- Sodhi, P., Kaess, M., Mukadam, M. and Anderson, S. (2021), 'Patchgraph: In-hand tactile tracking with learned surface normals', *CoRR abs/2111.07524*.  
**URL:** <https://arxiv.org/abs/2111.07524>
- Sundermeyer, M., Marton, Z.-C., Durner, M., Brucker, M. and Triebel, R. (2018), Implicit 3d orientation learning for 6d object detection from rgb images, in 'Proceedings of the European Conference on Computer Vision (ECCV)', pp. 699–715.
- Taylor, I., Dong, S. and Rodriguez, A. (2021), 'Gelslim3.0: High-resolution measurement of shape, force and slip in a compact tactile-sensing finger', *CoRR abs/2103.12269*.  
**URL:** <https://arxiv.org/abs/2103.12269>
- Tian, S., Ebert, F., Jayaraman, D., Mudigonda, M., Finn, C., Calandra, R. and Levine, S. (2019), Manipulation by

- feel: Touch-based control with deep predictive models, *in* '2019 International Conference on Robotics and Automation (ICRA)', IEEE, pp. 818–824.
- Wang, S., Wu, J., Sun, X., Yuan, W., Freeman, W. T., Tenenbaum, J. B. and Adelson, E. H. (2018), '3D Shape Perception from Monocular Vision, Touch, and Shape Priors', *ArXiv e-prints*.
- Yershova, A., Jain, S., Lavalley, S. M. and Mitchell, J. C. (2010), 'Generating uniform incremental grids on  $S^2$  using the hopf fibration', *The International journal of robotics research*.
- Yu, K.-T. and Rodriguez, A. (2018), Realtime state estimation with tactile and visual sensing. application to planar manipulation, *in* '2018 IEEE International Conference on Robotics and Automation (ICRA)', IEEE, pp. 7778–7785.
- Zeng, A., Song, S., Yu, K., Donlon, E., Hogan, F. R., Bauza, M., Ma, D., Taylor, O., Liu, M., Romo, E., Fazeli, N., Alet, F., Dafle, N. C., Holladay, R., Morona, I., Nair, P. Q., Green, D., Taylor, I. J., Liu, W., Funkhouser, T. A. and Rodriguez, A. (2018), Robotic pick-and-place of novel objects in clutter with multi-affordance grasping and cross-domain image matching, *in* 'IEEE International Conference on Robotics and Automation (ICRA)'.
- Zhou, Y., Barnes, C., Lu, J., Yang, J. and Li, H. (2018), 'On the continuity of rotation representations in neural networks', *CoRR* **abs/1812.07035**.  
**URL:** <http://arxiv.org/abs/1812.07035>

## A Contact shape prediction from tactile observations

Given a tactile observation, our goal is to extract the contact shape that produces it. To that aim, we train an image translation network (pix2pix) based on Isola et al. (2018) to map from RGB tactile observations to contact shapes, described below for completeness.

As shown in Figure 9, the input to the NN is an RGB tactile image of size  $160 \times 120 \times 3$ . The output corresponds to a binary contact mask of size  $160 \times 120 \times 3$ , which we flatten to  $160 \times 120$  to represent the contact shape.

The training data is collected autonomously in a controlled 4-axis stage that generates controlled touches on known 3D-printed shapes. In our case, we collect the calibration data from two 3D-printed boards with simple geometric shapes on them (see the top of Figure 9). From each controlled touch, we obtain a tactile observation and the pose of the board w.r.t. to the sensor. From this pose, we can later simulate the corresponding contact shape to the tactile observation using geometric contact rendering and the 3D model of the board.

Note that to do tactile localization on any object, we only need to gather calibration data once because the map between tactile observations and contact shapes is object-independent. Empirically, we find that the map is also independent of sensor instance.

The training input is a  $160 \times 240 \times 3$  image, consisting of the raw tactile image and the ground truth contact mask stitched together.

Both the generator and discriminator networks of the NN are in the form of convolution-BatchNorm-ReLu modules, as in Isola et al. (2018). The optimizer is Adam with an initial learning rate of 0.0002, that decays linearly. The momentum of Adam is 0.5. The GAN objective is the least squares loss function.

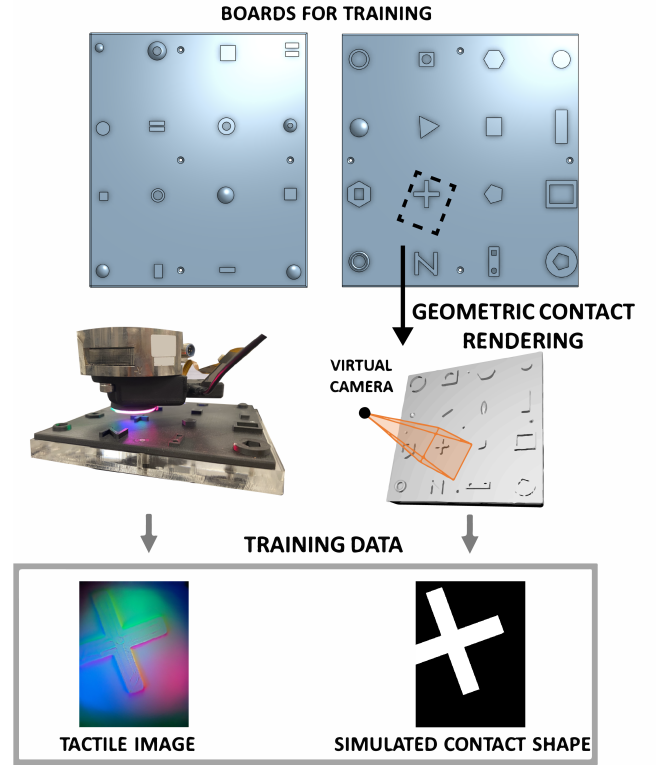
In practice, we collected 10,000 pairs of tactile observations in total (9,000 from the board at left, and 1,000 from the board at right), and trained the NN for 86 epochs.

## B Collecting ground-truth data for real objects

We collect labelled datasets of tactile observations of grasps on 20 objects mounted in known positions and orientations in the world. Each dataset contains pairs of RGB tactile images, and the corresponding ground-truth object pose relative to the gripper. This allows us to compute pose errors between Tac2Pose predictions from tactile observations, and the true calibrated object poses.

To get calibrated real pairs of contact poses and tactile observations, we first obtain a coarse estimate of the object pose using an overhead camera. We then refine that estimate using Tac2Pose for geometric contact rendering: we move the robot to our coarse estimate of the object pose, grasp the object, and compare the observed contact with the simulated contact shape in the estimated pose. We adjust the estimate of the object pose until the observed contact matches the simulated one.

The robotic system we use to collect the labelled datasets consists of a dual arm ABB Yumi with two WSG-32 grippers



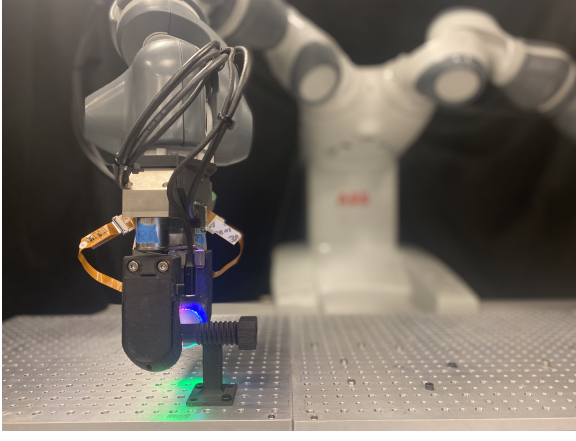
**Figure 9. Training data set-up to estimate real contact shapes from real tactile observations.** We use the boards at the top to collect real tactile observations from them as well as simulated contact shapes. By placing the boards on a robotic platform, we can move them w.r.t. the sensor to perform calibrated touches on them. From each touch, we recover both a tactile image and a simulated contact shape that we compute using the 3D model of the boards and its pose w.r.t the sensor when the touch happened.

and GelSlim 3.0 tactile sensing fingers. Figure 10 shows a still of the data collection procedure for the object stud.

We collect labelled observations of feasible grasps on each object. To determine which contacts should appear in the datasets, we first find the *stable poses* of each object. Stable poses are the poses that an object is most likely to fall in when dropped onto a table. We then determine a set of feasible grasp approach directions for each stable pose. We define the *grasp approach direction* as the axis of the grasp during a parallel jaw grasp. We break out the labelled datasets by grasp approach direction, to facilitate insight about what categories of grasps are easier to localize for different objects. For each grasp approach direction, we collect a set of equispaced observations, that correspond to a given grasp approach direction at various  $x, y$  locations relative to the object. In total, these observations correspond to the set of contacts that we are likely to encounter when picking up each object from a table.

## C Similarity metric for contact shapes

Given a new contact shape, we want to compare it to all pre-computed contact shapes in the grid to find what poses are more likely to produce it. To that aim, we use MOCO (He et al. 2019), a widely used tool in contrastive learning, to train a NN that encodes contact shapes into a low dimensional embedding allowing to compare them using the distance between their encodings.



**Figure 10. Collecting ground-truth data on real objects.** We 3D-print object models mounted on posts and fix them in known location relative to the robot. As a result, we can collect ground-truth data for test objects (the object stud is shown).

The NN encoder is a pre-trained ResNet-50 (He et al. 2016) cropped before the average-pooling layer to preserve spatial information. It encodes contact shapes into vectors of dimension 1000. To train, we use the same optimizer as He et al. (2019): stochastic gradient descent with a learning rate that starts at 0.03 and decays over time, momentum of 0.999, and no weight decay. Each training datapoint comes from selecting a random contact pose, rendering its contact shape, and finding its closest pose in the pre-computed grid. Then our input is the contact shape. The output or label is a vector with all entries zeros except the one that corresponds to the closest element that gets a one. This vector represents the probability of each poses in the grid to be the closest to the target pose. The loss function is the cross-entropy loss between the label and the softmax between the target encoder and the ones from the grid (see Fig. 3). As the NN gets trained, we recompute the encoding of the queue following (He et al. 2019). We train the models for 15 epochs, as they tend to overfit to simulated data after that.

To make the training data resemble more the real distribution of contact shapes, we train using as target contact shapes with different depth thresholds,  $\Delta d$ , selected randomly between 1 and 2 mm. This accounts for changes in the contact force applied to the sensor which can make contacts more or less deep (see Fig. 3). Finally, before encoding the contact shapes, we converted them into binary masks to ease the learning process and prevent that numerical mismatches between real and simulated contact shapes.

## D Multi-contact for N sensors

To derive Equation 1 in Section 3.4, we will prove a more general equation for the object pose  $x$  when it is in contact with N sensors:

$$P(x|C_1, \dots, C_N) = \frac{P(x|C_1) \cdot \dots \cdot P(x|C_N) \cdot P_{ta}(x)/P_{tr}(x)^N}{\sum_{x'} P(x'|C_1) \cdot \dots \cdot P(x'|C_N) \cdot P_{ta}(x')/P_{tr}(x')^N} \quad (2)$$

where  $P(x|C_i)$  is the likelihood that pose  $x$  has produced a contact shape  $C_i$  on sensor  $i$ .  $P_{ta}(x)$  is a prior over all the possible contact poses that would result in contact with the N sensors in the current task.  $P_{tr}(x)$  is the distribution

over the contact poses used to train the similarity function in Section 3.1.

Next, we prove Equation (2). Assuming that we have access to the poses of N sensors, given an object pose  $x$ , the contact shapes  $\{C_i\}$  become determined. This allows us to write the joint distribution of pose and contact shapes as:

$$P(x, C_1, \dots, C_N) = P_{ta}(x) \cdot P(C_1|x) \cdot \dots \cdot P(C_N|x) \quad (3)$$

Now we can use Bayes theorem on the  $P(C_i|x)$  terms:

$$P(C_i|x) = P(x|C_i) \cdot P(C_i)/P_{tr}(x) \quad (4)$$

and obtain:

$$P(x, C_1, \dots, C_N) = P(x|C_1) \cdot P(C_1) \cdot \dots \cdot P(x|C_N) \cdot P(C_N) \cdot P_{ta}(x)/P_{tr}(x)^N \quad (5)$$

where we take into account that the  $P(x|C_i)$  have been trained using a predefined distribution of poses  $P_{tr}(x)$  that does not necessarily match  $P_{ta}(x)$ . Now, we can compute  $P(x|C_1, \dots, C_N)$  using again the Bayes theorem:

$$P(x|C_1, \dots, C_N) = \frac{P(x, C_1, \dots, C_N)}{P(C_1, \dots, C_N)} = \frac{P(x, C_1, \dots, C_N)}{\sum_{x'} P(x', C_1, \dots, C_N)} \quad (6)$$

and thus

$$P(x|C_1, \dots, C_N) = \frac{(\prod_i^N P(x|C_i) \cdot P(C_i)) \cdot P_{ta}(x)/P_{tr}(x)^N}{\sum_{x'} (\prod_i^N P(x'|C_i) \cdot P(C_i)) \cdot P_{ta}(x')/P_{tr}(x')^N} \quad (7)$$

We can now cancel the terms  $P(C_i)$  that appear both in the numerator and denominator, getting:

$$P(x|C_1, \dots, C_N) = \frac{(\prod_i^N P(x|C_i)) \cdot P_{ta}(x)/P_{tr}(x)^N}{\sum_{x'} (\prod_i^N P(x'|C_i)) \cdot P_{ta}(x')/P_{tr}(x')^N} \quad (8)$$

This concludes the proof of Equation (2). In practice, we discretize the set of contact poses  $\{x\}$  that result in contact with the N sensors using the grid over of sensor 1 (this is an arbitrary choice). Then, we use the transformation between sensor 1 and sensor  $i$  to compute each  $P(x|C_i)$  using the closest pose to  $x$  in the grid of sensor  $i$ . Note that often a pose that results in contact with sensor 1 will not contact sensor  $i$ . In that case, we do not consider that pose as we are only interested in poses that contact the N sensors. Finally, because the grids are dense and structured, finding the closest pose to  $x$  in a grid has a minor effect on performance and is fast to compute.

We can use Equation (2) to derive Equation (1) in Section 3.4 under two extra assumptions. First, we observe
















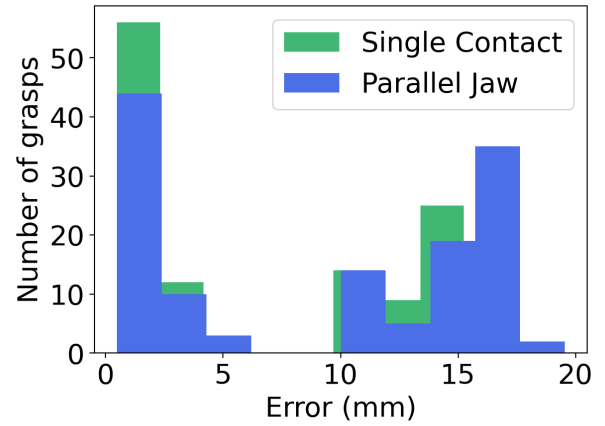
that the denominator is constant because all contact shapes  $C_i$  are given. Next, if we have no prior over the contact poses during training, then  $P_{tr}(x)$  is constant, and that leads to Equation 1 repeated here for completeness:

$$P(x|C_1, \dots, C_N) \propto P(x|C_1) \cdot \dots \cdot P(x|C_N) \cdot P_{ta}(x) \quad (9)$$

## E Results by grasp approach direction

**Table 6.** Results by grasp approach direction for Parallel Jaw ablation of Tac2Pose

		Grasp Approach Direction mm (norm)			
		1	2	3	4
Long Grease		1.2 (0.0)	9.9 (0.3)		
Grease		0.8 (0.1)	2.0 (0.2)		
Stud		13.6 (0.3)	13.2 (0.3)		
Pin		5.5 (0.2)	5.7 (0.2)		
Hanger		2.7 (0.1)	1.1 (0.0)	1.3 (0.0)	6.2 (0.2)
Hydraulic		9.1 (0.4)	1.7 (0.1)		
Hose		46.1 (0.7)	37.2 (0.6)		
Round Hose		35.2 (0.7)	38.9 (0.7)		
Holder		2.0 (0.1)	2.9 (0.1)		
Round Cable		15.2 (0.8)	2.2 (0.1)		
Couple		13.9 (0.6)	19.6 (0.7)	21.4 (0.8)	
Round Couple		4.8 (0.2)	14.8 (0.6)	17.8 (0.7)	
Cable Clip		10.6 (0.6)	12.1 (0.7)		



**Figure 11.** Distribution of errors for single contact vs. parallel jaw contact case for round clip.

## F Round clip discussion

Our error metric - median error of the best match - does not capture the error distributions for round clip well. As discussed in Section 4.2 and tabulated in Table 6, round clip is much easier to localize from one grasp approach direction than the other. This results in similar, bimodal error distributions in both the single contact and parallel jaw contact cases, as seen in Figure 11. Instead, we compare the means of the two distributions and observe the underlying similarity between the two distributions more clearly: the mean error of the best match in the single contact case is 7.6 mm, compared with 9.2 mm in the parallel jaw contact case.